IEEE Access
Multidisciplinary | Rapid Review | Open Access Journal

Received July 29, 2019, accepted August 8, 2019, date of publication August 19, 2019, date of current version August 30, 2019.

Digital Object Identifier 10.1109/ACCESS.2019.2935989

Synchronization and Stability of Two Pairs of Reversed Rotating Exciters Mounted on Two Different Rigid Frames

XUELIANG ZHANG[1,2], ZHIHUI WANG[1], YUNPENG ZHU[3], JINLIN XU[1], AND BANG-CHUN WEN[1]

[1]School of Mechanical Engineering and Automation, Northeastern University, Shenyang 110819, China
[2]State Key Laboratory of Tunnel Boring Machine, Northern Heavy Industries Group, Shenyang 110141, China
[3]Department of Automatic Control and Systems Engineering, University of Sheffield, Sheffield S10 2TN, U.K.

Corresponding author: Xueliang Zhang (luckyzxl7788@163.com)

This work was supported in part by the National Natural Science Foundations of China under Grant 51675090, in part by the Fundamental Research Funds for the Central Universities under Grant N170304013, and in part by the China Postdoctoral Science Foundation under Grant 2017M621145.

ABSTRACT Usually, the synchronization studies of two or multiple exciters are focused on the single rigid frame (RF), but that mounted on different RFs is still a problem in engineering practice. This study attempts to solve this issue by considering a dynamical model with double RFs including two pairs of exciters, in which each pair of exciters is distributed on different RFs. The synchronous and stable states of the system in different resonant regions are discussed in detail in present work. First, the mathematical modeling of the system is carried out, and the relative motion differential equations of two RFs and their responses are achieved by using the transfer function method. Then, the theoretical conditions of implementing synchronization and stability of the system are derived. The coupling dynamic characteristics of the system, including frequency-amplitude relationships, coupling torques, stable phase differences, synchronization and stability abilities, and the phenomenon of the diversity of nonlinear system, are numerically investigated. Finally, simulations are performed by using the Runge-Kutta method to validate the theoretical and numerical characteristic analysis results. In the sub-resonant region with respect to the natural frequency with regard to the relative motion between two RFs, the stronger and more stable positive superposition of vibration amplitude between two RFs can be realized, which is the desire in engineering.

INDEX TERMS Synchronization, stability, exciters, resonant, motor.

I. INTRODUCTION

As a special nonlinear phenomenon, synchronization often appears in human society and industrial production processes, such as complex networks, pendulum clocks, electromechanical devices, chemical and mechanical oscillators, etc. [1]–[5].

In most cases, synchronization phenomenon is harmful and unexpected in practice, for example, soldiers are forbidden to march synchronously when passing a wire bridge, because a resonant response can be activated by the synchronous walking that may cause a disaster. So the studies on dynamic vibration absorbers [6], [7] have been attracting the attentions of many scholars in order to reduce the synchronous resonant responses.

However, from the point of views of other aspects, synchronization can be utilized beneficially. For example, in the radio broadcast, the receiving frequency must match the transmitting frequency, which is known as the send-receive synchronization, in order to receive the expected sounds from radio stations [12]. Another typical representative of applying synchronization in engineering practice is the synchronization of exciters (generally related to be as unbalanced rotors separately driven by induced motors), which has been widely investigated and applied to various industry production process with different kinds of vibrating

The associate editor coordinating the review of this article and approving it for publication was Hassan Ouakad.

equipments for vibratory crushing, feeding, conveying, screening, separating, cooling, drying, dewatering, etc. These devices can not only improve the performances of the industry process, but also enhance the production efficiency.

For synchronization of exciters in the vibrating systems, the most noteworthy researches were those given by Blekhman [8]–[11], who firstly explored the synchronization principle of two identical exciters by using Poincare's small parameter method. After that, Wen *et al.* [12] successfully implemented such theory to engineering practice and established a branch of learning known as the vibration utilization engineering. In addition, the synchronization of two (or four) non-ideal exciters supported by a flexible portal frame structure was proposed by Balthazar *et al.* [13], [14], where a special phenomenon called ''Sommerfeld effect'' was studied, and Fang and Hou [15] investigated the synchronization characteristics of rotor-pendula systems driven by two exciters. Recently, the synchronization and stability of three or four homodromy exciters in a vibrating system with the single RF [16], [17], as well as that of two exciters in a nonlinear vibrating system with double RFs [18], have been studied. Considering the effect of the drying friction, synchronous operation of a cylindrical roller in a vibrating cavity driven by two exciters is discussed in theory and experiments [19].

In the abovementioned works, synchronization theory of exciters has been extensively studied, these works mainly focus on synchronization problem under the precondition that all relevant exciters are mounted on the same RF, but the coupling mechanism and synchronization principles of multiple exciters which is respectively mounted on different RFs, are seldom considered. Therefore, it is necessary to deeply explore their stabilities of the synchronous states, especially under different resonant regions of the vibrating system with multiple RFs.

To resolve the above issues, a double RFs dynamical model with two pairs of exciters is discussed in this study, where each pair of reversed rotating exciters is mounted on different RFs. The synchronous and stable states of two pairs of exciters under different resonant conditions will be discussed, as well as the corresponding relative motion relationship between two RFs. The related research results are expected to offer a guidance for the design of new vibrating machines, especially for a certain type of vibrating crushers.

This paper is organized as follows: In section II, the dynamic model of the system is introduced and the mathematical modeling of the system is derived. The responses and natural frequencies of the system are given in section III. Section IV is dedicated to theoretically derive the conditions of synchronization and stability. The coupling dynamic characteristics of the system are numerically discussed in section V. Simulations are provided to validate the proposed theoretical results in section VI. Finally, conclusions are summarized.

II. DESCRIPTION OF THE SYSTEM AND MATHEMATICAL MODELING

A. NOMENCLATURE

f_{0i}	damping coefficient of axes of the induction motor i, i =1, 2, 3, 4
f_{jx}	damping constant of RF j in x-direction, $j = 1, 2$
k_{jx}	stiffness of spring j in x-direction, $j = 1, 2$
m_j	mass of RF j, $j = 1, 2$
m_0	mass of the standard exciter, which is the exciter mounted on RF1, i.e., $m_{01} = m_0$
m_{0i}	mass of the exciter i, i =1, 2, here two exciters mounted on RF1 are identical, denoted by m_{01}, as well as those on RF2 denoted by m_{02}
m	induced mass of the vibrating system
M_1	mass of RF1 including two exciters, $M_1 = m_1 + 2m_{01}$
M_2	mass of RF2 including two exciters, $M_2 = m_2 + 2m_{02}$
M	mass of the total vibrating system, $M = M_1 + M_2$
r_i	eccentric radius of the exciter i, $r_i = r$, i =1, 2
r_{m1}	mass ratio of the standard exciter to RF1, $r_{\mathrm{m1}} = m_0/M_1$
r_{m2}	mass ratio of the standard exciter to RF2, $r_{\mathrm{m2}} = m_0/M_2$
T_{ei}	electromagnetic torque of the induction motor i, i =1, 2, 3, 4
T_{e0i}	electromagnetic torque of the induction motor i operating steadily at the angular velocity ω_{m0}, i =1, 2, 3, 4
z_i	ratio of frequency between the operating frequency and natural frequencies, $z_i = \omega_{\mathrm{m0}}/\omega_i$
ω_{m0}	average angular velocity of four exciters in the steady-state
ω_2	natural frequency of RF2, $\omega_2 = \sqrt{(k_{1x} + k_{2x})/M_2}$
ω_0	natural frequency of the main vibrating system, $\omega_0 = \sqrt{k_{1x}/m}$
ω_g	natural frequency of the isolated vibrating system, $\omega_g = \sqrt{k_{2x}/m}$
ξ_{1x}	equivalently critical damping ratio of relative motion between two RFs in x-direction, $\xi_{1x} \leq 0.07$, for a vibrating system with small damping
ξ_{2x}	critical damping ratio of RF2 in x-direction
η	ratio of mass between the exciters mounted on RF2 and the standard exciter, $\eta = m_{02}/m_0$
$(\dot{\bullet})$	$\mathrm{d}\bullet/\mathrm{d}t$
$(\ddot{\bullet})$	$\mathrm{d}^2\bullet/\mathrm{d}t^2$

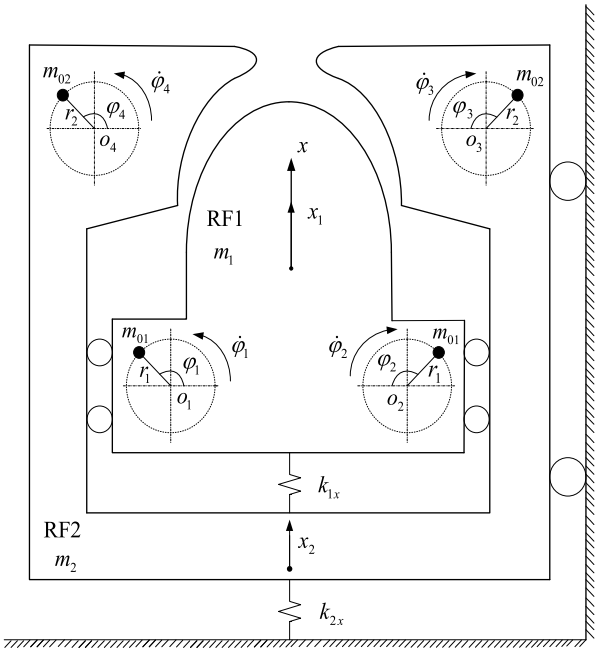

FIGURE 1. Dynamical model of the vibrating system under study.

Figure 1 shows a dynamical model of the vibrating system under study, which mainly includes two RFs, springs and two pairs of reversed rotating exciters mounted respectively on two different RFs, where each exciter is driven by induction motor. The RF1 is nested inside the RF2 (displayed by RF1 and RF2 in Fig. 1), the masses of these two RFs are denoted by m_1 and m_2, respectively, and they are connected by spring of the main vibrating system k_{1x}, the RF2 is also linked with foundation by spring of the isolative system k_{2x}. Two pairs of exciters are driven by the induction motors separately, two identical exciters rotating in reversed directions are mounted on the same RF, and the mass and eccentric radius of two exciters on RF1 are identical, denoted by m_{01} and r_1. Similarly, those on RF2 are denoted by m_{02} and r_2, see Fig. 1. The spin axes centers of the exciters are denoted by o_i $(i = 1, 2, 3, 4)$, and their rotating phases are φ_i $(i = 1, 2, 3, 4)$, respectively. The motions of RF1 and RF2 along with x-direction are denoted by x_1 and x_2.

According to the derivation process in [16], based on Lagrange's equation, the mathematical modeling of the vibrating system is directly derived as follows:

$$\begin{aligned}
&M_1\ddot{x}_1 + f_{1x}(\dot{x}_1 - \dot{x}_2) + k_{1x}(x_1 - x_2) \\
&\quad = \sum_{i=1}^{2} m_{01} r_1 (\dot{\varphi}_i^2 \sin\varphi_i - \ddot{\varphi}_i \cos\varphi_i) \\
&M_2\ddot{x}_2 - f_{1x}\dot{x}_1 + (f_{1x} + f_{2x})\dot{x}_2 - k_{1x}x_1 + (k_{1x} + k_{2x})x_2 \\
&\quad = \sum_{i=3}^{4} m_{02} r_2 (\dot{\varphi}_i^2 \sin\varphi_i - \ddot{\varphi}_i \cos\varphi_i) \\
&J_{01}\ddot{\varphi}_1 + f_{01}\dot{\varphi}_1 = T_{e1} - m_{01} r_1 \ddot{x}_1 \cos\varphi_1 \\
&J_{02}\ddot{\varphi}_2 + f_{02}\dot{\varphi}_2 = T_{e2} - m_{01} r_1 \ddot{x}_1 \cos\varphi_2 \\
&J_{03}\ddot{\varphi}_3 + f_{03}\dot{\varphi}_3 = T_{e3} - m_{02} r_2 \ddot{x}_2 \cos\varphi_3 \\
&J_{04}\ddot{\varphi}_4 + f_{04}\dot{\varphi}_4 = T_{e4} - m_{02} r_2 \ddot{x}_2 \cos\varphi_4
\end{aligned} \tag{1}$$

where $M_1 = m_1 + 2m_{01}$, $M_2 = m_2 + 2m_{02}$, $M = M_1 + M_2$, $J_{01} = J_{02} = m_{01} r_1^2$, $J_{03} = J_{04} = m_{02} r_2^2$, $r_1 = r_2 = r$, and the description of the other parameters can be seen in Nomenclature.

III. RESPONSES AND NATURAL FREQUENCIES OF THE VIBRATING SYSTEM

For the convenience of deducing the responses and natural frequencies, we denote $m_{01} = m_0$, $m_{02} = \eta m_0$ $(\eta > 0)$, and φ is the average phase of four exciters, where $\varphi_1 + \varphi_2 + \varphi_3 + \varphi_4 = 4\varphi$, the phase differences of four exciters are denoted by $\varphi_1 - \varphi_2 = 2\alpha_1$, $\varphi_3 - \varphi_4 = 2\alpha_2$, and $\varphi_2 - \varphi_3 = 2\alpha_3$, respectively, such that

$$\begin{aligned}
\varphi_1 &= \varphi + \frac{3}{2}\alpha_1 + \frac{1}{2}\alpha_2 + \alpha_3 = \varphi + \nu_1 \\
\varphi_2 &= \varphi - \frac{1}{2}\alpha_1 + \frac{1}{2}\alpha_2 + \alpha_3 = \varphi + \nu_2 \\
\varphi_3 &= \varphi - \frac{1}{2}\alpha_1 + \frac{1}{2}\alpha_2 - \alpha_3 = \varphi + \nu_3 \\
\varphi_4 &= \varphi - \frac{1}{2}\alpha_1 - \frac{3}{2}\alpha_2 - \alpha_3 = \varphi + \nu_4
\end{aligned} \tag{2}$$

During the steady operation process of the system, if two pairs of exciters can operate synchronously, their synchronous angular velocity is given as $\dot{\varphi} = \omega_{m0}$.

In order to analyze the relative motion between two RFs, based on [12], the relationships between the acceleration and the displacement can be obtained as

$$\ddot{x}_1 = -\omega_{m0}^2 x_1, \quad \ddot{x}_2 = -\omega_{m0}^2 x_2 \tag{3}$$

When two pairs of exciters operate synchronously in the steady state, their average angular acceleration is zero (i.e., $\ddot{\varphi} = 0$). Moreover, f_{2x} in (1) can be ignored (generally in engineering, compared with the damping of the main vibrating system f_{1x}, that of the isolative system f_{2x} is so small that it might be neglected [12]), substituting (3) into the first two formulae of (1), there are

$$\begin{aligned}
&M_1'\ddot{x}_1 + f_{1x}(\dot{x}_1 - \dot{x}_2) + k_{1x}(x_1 - x_2) \\
&\quad = m_0 r \omega_{m0}^2 [\sin(\varphi + \nu_1) + \sin(\varphi + \nu_2)]
\end{aligned} \tag{4}$$

$$\begin{aligned}
&M_2'\ddot{x}_2 - f_{1x}(\dot{x}_1 - \dot{x}_2) - k_{1x}(x_1 - x_2) \\
&\quad = \eta m_0 r \omega_{m0}^2 [\sin(\varphi + \nu_3) + \sin(\varphi + \nu_4)]
\end{aligned} \tag{5}$$

where $M_1' = M_1$ and $M_2' = M_2 - k_{2x}/\omega_{m0}^2 \approx M_2$, due to the fact that in engineering, the value of k_{2x}/ω_{m0}^2, which is usually less than k_{1x}/ω_{m0}^2 [12], is quite small and can be neglected compared with M_2.

In the steady state, since the synchronous angular velocity of two pairs of exciters satisfies $\dot{\varphi} = \omega_{m0}$, arranging Eqs. (4)

and (5) by the treatment of (4) $\times$ $(M_2^{'}/M_1^{'}+M_2^{'})$ $-$ (5) $\times$ $(M_1^{'}/M_1^{'}+M_2^{'})$,the differential equation of relative motion between two RFs can be deduced as

$$\begin{aligned} m\ddot{x}_{12}+f_{1x}\dot{x}_{12}+k_{1x}x_{12} &= \frac{M_2^{'}}{M_1^{'}+M_2^{'}}m_0r\omega_{\mathrm{m0}}^2\sum_{i=1}^{2}\sin(\varphi+\nu_i) \\ &\quad -\frac{M_1^{'}}{M_1^{'}+M_2^{'}}\eta m_0r\omega_{\mathrm{m0}}^2\sum_{i=3}^{4}\sin(\varphi+\nu_i) \end{aligned} \tag{6}$$

with

$$m=\frac{M_1^{'}M_2^{'}}{M_1^{'}+M_2^{'}},\quad \ddot{x}_{12}=\ddot{x}_1-\ddot{x}_2,\ \dot{x}_{12}=\dot{x}_1-\dot{x}_2,\ x_{12}=x_1-x_2$$

where m is defined as the induced mass of the vibrating system, and x_{12}, $\dot{x}_{12}$ and $\ddot{x}_{12}$ are relative displacement, velocity and acceleration between two RFs, respectively.

The natural frequency ω_0 and the response of (6) can be directly obtained as

$$\omega_0=\sqrt{\frac{k_{1x}}{m}}=\sqrt{\frac{k_{1x}(M_1^{'}+M_2^{'})}{M_1^{'}M_2^{'}}} \tag{7}$$

and

$$\begin{aligned} x_{12}=&A_{12}^{'}[\sin(\varphi+\nu_1-\gamma_{12})+\sin(\varphi+\nu_2-\gamma_{12})] \\ &-\eta A_{12}^{''}[\sin(\varphi+\nu_3-\gamma_{12})+\sin(\varphi+\nu_4-\gamma_{12}] \end{aligned} \tag{8}$$

where ω_0 is the frequency allowing the amplitude of the relative motion to reach the maximum value, and

$$A_{12}^{'}=\frac{r_{\mathrm{m1}}z_0^2r}{\sqrt{(1-z_0^2)^2+(2\xi_{1x}z_0)^2}}$$

$$A_{12}^{''}=\frac{r_{\mathrm{m2}}z_0^2r}{\sqrt{(1-z_0^2)^2+(2\xi_{1x}z_0)^2}}=\frac{M_1}{M_2}A_{12}^{'},$$

$$\gamma_{12}=\arctan\left(\frac{2\xi_{1x}z_0}{1-z_0^2}\right),\quad z_0=\frac{\omega_{\mathrm{m0}}}{\omega_0},\ r_{\mathrm{m1}}=\frac{m_0}{M_1^{'}}\approx\frac{m_0}{M_1},$$

$$r_{\mathrm{m2}}=\frac{m_0}{M_1^{'}}\approx\frac{m_0}{M_1},\quad \xi_{1x}=\frac{f_{1x}}{2\sqrt{k_{1x}m}}.$$

According to (2), the response amplitude of the relative motion between two RFs in the steady state, denoted by λ_{12}, is directly obtained as

$$\begin{aligned} &\lambda_{12} \\ &=A_{12}^{'}\sqrt{\begin{array}{l} 2+2\left(\eta\dfrac{M_1}{M_2}\right)^2+2\cos 2\alpha_1+2\left(\eta\dfrac{M_1}{M_2}\right)^2\cos 2\alpha_2 \\ -2\eta\dfrac{M_1}{M_2}\cos 2\alpha_3-2\eta\dfrac{M_1}{M_2}\cos(2\alpha_1+2\alpha_3) \\ -2\eta\dfrac{M_1}{M_2}\cos(2\alpha_2+2\alpha_3) \\ -2\eta\dfrac{M_1}{M_2}\cos(2\alpha_1+2\alpha_3+2\alpha_3) \end{array}} \end{aligned} \tag{9}$$

The above discussions are mainly focused on the relative motion between two RFs. However, the absolute motions x_1 and x_2 are also important [18], which are investigated as follows.

Based on the first two formulae of (1), the responses of two RFs can be solved by the transfer function method [18] as

$$\begin{aligned} x_1=&F_1r[\sin(\varphi+\nu_1-\gamma_{1x})+\sin(\varphi+\nu_2-\gamma_{1x})] \\ &+\eta F_3r[\sin(\varphi+\nu_3-\gamma_{3x})+\sin(\varphi+\nu_4-\gamma_{3x})] \\ x_2=&F_2r[\sin(\varphi+\nu_1-\gamma_{2x})+\sin(\varphi+\nu_2-\gamma_{2x})] \\ &+\eta F_4r[\sin(\varphi+\nu_3-\gamma_{4x})+\sin(\varphi+\nu_4-\gamma_{4x})] \end{aligned} \tag{10}$$

where the detailed expressions of (10) are presented in Appendix A.

According to (10), during the process of the steady operation of the system, the response amplitudes of two RFs in x-direction, denoted by λ_1 and λ_2, can be expressed by

$$\begin{aligned} \lambda_1&=\sqrt{A_1^2+B_1^2} \\ \lambda_2&=\sqrt{C_1^2+D_1^2} \end{aligned} \tag{11}$$

and the specific expressions of A_1, B_1, C_1 and D_1 are listed in Appendix B.

In order to calculate all natural frequencies of the system, based on the first two formulae of (1), the inertial and stiffness couplings of the system can be written in the matrix form.

$$\begin{aligned} \mathbf{M}&=\begin{pmatrix} M_1 & 0 \\ 0 & M_2 \end{pmatrix},\quad \mathbf{K}=\begin{pmatrix} k_{1x} & -k_{1x} \\ -k_{1x} & k_{1x}+k_{2x} \end{pmatrix} \\ \Delta(\omega_{\mathrm{m0}}^2)&=\begin{vmatrix} k_{1x}-\omega_{\mathrm{m0}}^2M_1 & -k_{1x} \\ -k_{1x} & k_{1x}+k_{2x}-\omega_{\mathrm{m0}}^2M_2 \end{vmatrix} \end{aligned} \tag{12}$$

where $\mathbf{M}$ is the inertia coupling matrix, $\mathbf{K}$ is the stiffness coupling matrix, and $\Delta(\omega_{\mathrm{m0}}^2)$ denotes the characteristic equation of eigenvalues of the system.

Let $\Delta(\omega_{\mathrm{m0}}^2)=0$, there is

$$\begin{aligned} \omega_{\mathrm{m0}}^4M_1M_2-\omega_{\mathrm{m0}}^2M_1k_{1x}-\omega_{\mathrm{m0}}^2M_1k_{2x} \\ -\omega_{\mathrm{m0}}^2M_2k_{1x}+k_{1x}k_{2x}=0 \end{aligned} \tag{13}$$

Solving (13), the natural frequencies of the system in x-direction, denoted by ω_{inv} and ω_{sam}, are expressed as

$$\begin{aligned} \omega_{\mathrm{inv}}&=\sqrt{\frac{M_1k_{1x}+M_1k_{2x}+M_2k_{1x}+\sqrt{\begin{array}{l}(M_2k_{1x}+M_1k_{1x})^2 \\ +M_1k_{2x}(M_1k_{2x}+2M_1k_{1x}-2M_2k_{1x})\end{array}}}{2M_1M_2}} \\ \omega_{\mathrm{sam}}&=\sqrt{\frac{M_1k_{1x}+M_1k_{2x}+M_2k_{1x}-\sqrt{\begin{array}{l}(M_2k_{1x}+M_1k_{1x})^2 \\ +M_1k_{2x}(M_1k_{2x}+2M_1k_{1x}-2M_2k_{1x})\end{array}}}{2M_1M_2}} \end{aligned} \tag{14}$$

In engineering practice, the stiffness of the isolative vibrating system k_{2x} is far smaller than that of the main vibrating system k_{1x} ($k_{2x}<<k_{1x}$) [12], [18]. Hence k_{2x} of ω_{inv} can be ignored as $k_{2x}=0$, thus we have $\omega_{\mathrm{inv}}\approx\omega_0$, which enables one to know that ω_{inv} corresponds to the natural frequency of the main vibrating system.

Further discussions on the response and natural frequencies characteristics of the system will be conducted in the following studies by using numerical analysis method.

IV. SYNCHRONIZATION OF THE VIBRATING SYSTEM

A. SYNCHRONIZATION CONDITIONS

When two pairs of exciters operate synchronously, differentiating (10) to get $\ddot{x}_1$ and $\ddot{x}_2$, inserting them into the last four formulae of (1), and over one period $\varphi = 0 \sim 2\pi$ the integration is made, the mean is taken, then the average balanced equations of two pairs of exciters, can be obtained as follows

$$T_{e0i} - f_{0i}\omega_{\mathrm{m}0} = \bar{T}_{Li}, \quad i = 1, 2, 3, 4 \tag{15}$$

Here $\bar{T}_{Li}(i = 1, 2, 3, 4)$ represent the load torques of motor i, which are expressed as follows

$$\begin{aligned}
\overline{T}_{L1} &= T_uF_1[\sin\gamma_{1x}+\cos(2\overline{\alpha}_1)\sin\gamma_{1x} + \sin(2\overline{\alpha}_1)\cos\gamma_{1x}] \\
&\quad + \eta T_uF_2[\cos(2\overline{\alpha}_1 + 2\overline{\alpha}_2 + 2\overline{\alpha}_3)\sin\gamma_{2x} \\
&\quad + \cos(2\overline{\alpha}_1 + 2\overline{\alpha}_3)\sin\gamma_{2x} + \sin(2\overline{\alpha}_1 + 2\overline{\alpha}_2 \\
&\quad + 2\overline{\alpha}_3)\cos\gamma_{2x} + \sin(2\overline{\alpha}_1 + 2\overline{\alpha}_3)\cos\gamma_{2x}] \\
\overline{T}_{L2} &= T_uF_1[\sin\gamma_{1x}+\cos(2\overline{\alpha}_1)\sin\gamma_{1x} \\
&\quad - \sin(2\overline{\alpha}_1)\cos\gamma_{1x}] + \eta T_uF_2[\cos(2\overline{\alpha}_1 \\
&\quad + 2\overline{\alpha}_3)\sin\gamma_{2x} + \cos(2\overline{\alpha}_3)\sin\gamma_{2x} \\
&\quad + \sin(2\overline{\alpha}_3)\cos\gamma_{2x} + \sin(2\overline{\alpha}_1 + 2\overline{\alpha}_3)\cos\gamma_{2x}] \\
\overline{T}_{L3} &= \eta^2 T_uF_4[\sin\gamma_{4x} + \cos(2\overline{\alpha}_2)\sin\gamma_{4x} \\
&\quad + \sin(2\overline{\alpha}_2)\cos\gamma_{4x}] + \eta T_uF_2[\cos(2\overline{\alpha}_1 \\
&\quad + 2\overline{\alpha}_3)\sin\gamma_{2x} + \cos(2\overline{\alpha}_3)\sin\gamma_{2x} \\
&\quad - \sin(2\overline{\alpha}_1 + 2\overline{\alpha}_3)\cos\gamma_{2x} - \sin(2\overline{\alpha}_3)\cos\gamma_{2x}] \\
\overline{T}_{L4} &= \eta^2 T_uF_4[\sin\gamma_{4x} + \cos(2\overline{\alpha}_2)\sin\gamma_{4x} \\
&\quad + \sin(2\overline{\alpha}_2)\cos\gamma_{4x}] + \eta T_uF_2[\cos(2\overline{\alpha}_1 + 2\overline{\alpha}_2 \\
&\quad + 2\overline{\alpha}_3)\sin\gamma_{2x} + \cos(2\overline{\alpha}_2 + 2\overline{\alpha}_3)\sin\gamma_{2x} \\
&\quad - \sin(2\overline{\alpha}_2 + 2\overline{\alpha}_3)\cos\gamma_{2x} \\
&\quad - \sin(2\overline{\alpha}_1 + 2\overline{\alpha}_2 + 2\overline{\alpha}_3)\cos\gamma_{2x}]
\end{aligned} \tag{16}$$

where $T_u = m_0r^2\omega_{\mathrm{m}0}^2/2$ is the kinetic energy of the standard exciter, and the detailed expressions of (16) are given in Appendix C.

It should be noted that during the process of aforementioned integration for obtaining (15), since the changes of $2\alpha_i$ (i =1, 2, 3) are much smaller than $\varphi(\dot{\varphi} = \omega_{\mathrm{m}0})$ for time t, they can be referred to as the slow changing parameter [8]–[11]. Hence, $2\alpha_i$ can be replaced by their average value $2\bar{\alpha}_i$.

According to (16), the differences of output electromagnetic torques between any two motors are expressed as

$$\begin{aligned}
\Delta T_{012} &= \overline{T}_{L1} - \overline{T}_{L2} \\
&= 2T_uF_1\sin(2\overline{\alpha}_1)\cos\gamma_{1x} + \eta T_uF_2[\cos(2\overline{\alpha}_1 \\
&\quad + 2\overline{\alpha}_2 + 2\overline{\alpha}_3)\sin\gamma_{2x} + \cos(2\overline{\alpha}_1 \\
&\quad + 2\overline{\alpha}_3)\sin\gamma_{2x} - \cos(2\overline{\alpha}_2 + 2\overline{\alpha}_3)\sin\gamma_{2x} \\
&\quad - \cos(2\overline{\alpha}_3)\sin\gamma_{2x} + \sin(2\overline{\alpha}_1 + 2\overline{\alpha}_2 \\
&\quad + 2\overline{\alpha}_3)\cos\gamma_{2x} - \sin(2\overline{\alpha}_3)\cos\gamma_{2x} \\
&\quad + \sin(2\overline{\alpha}_1 + 2\overline{\alpha}_3)\cos\gamma_{2x} \\
&\quad - \sin(2\overline{\alpha}_2 + 2\overline{\alpha}_3)\cos\gamma_{2x}] \\
\Delta T_{023} &= \overline{T}_{L2} - \overline{T}_{L3} \\
&= T_uF_1[\sin\gamma_{1x} + \cos(2\overline{\alpha}_1)\sin\gamma_{1x} \\
&\quad - \sin(2\overline{\alpha}_1)\cos\gamma_{1x}] - \eta^2 T_uF_4[\sin\gamma_{4x} \\
&\quad + \cos(2\overline{\alpha}_2)\sin\gamma_{4x} + \sin(2\overline{\alpha}_2)\cos\gamma_{4x}] \\
&\quad + \eta T_uF_2[\cos(2\overline{\alpha}_2 + 2\overline{\alpha}_3)\sin\gamma_{2x} \\
&\quad - \cos(2\overline{\alpha}_1 + 2\overline{\alpha}_3)\sin\gamma_{2x} \\
&\quad + \sin(2\overline{\alpha}_1 + 2\overline{\alpha}_3)\cos\gamma_{2x} \\
&\quad + \sin(2\overline{\alpha}_2 + 2\overline{\alpha}_3)\cos\gamma_{2x} + 2\sin(2\overline{\alpha}_3)\cos\gamma_{2x}] \\
\Delta T_{034} &= \overline{T}_{L3} - \overline{T}_{L4} \\
&= 2\eta^2 T_uF_4\sin(2\overline{\alpha}_2)\cos\gamma_{4x} \\
&\quad + \eta T_uF_2[\cos(2\overline{\alpha}_1 + 2\overline{\alpha}_3)\sin\gamma_{2x} \\
&\quad + \cos(2\overline{\alpha}_3)\sin\gamma_{2x} - \cos(2\overline{\alpha}_1 + 2\overline{\alpha}_2 \\
&\quad + 2\overline{\alpha}_3)\sin\gamma_{2x} - \cos(2\overline{\alpha}_2 + 2\overline{\alpha}_3)\sin\gamma_{2x} \\
&\quad - \sin(2\overline{\alpha}_3)\cos\gamma_{2x} + \sin(2\overline{\alpha}_1 + 2\overline{\alpha}_2 \\
&\quad + 2\overline{\alpha}_3)\cos\gamma_{2x} + \sin(2\overline{\alpha}_1 + 2\overline{\alpha}_3)\cos\gamma_{2x} \\
&\quad - \sin(2\overline{\alpha}_2 + 2\overline{\alpha}_3)\cos\gamma_{2x}] \\
\Delta T_{013} &= \overline{T}_{L1} - \overline{T}_{L3} \\
&= T_uF_1[\sin\gamma_{1x} + \cos(2\overline{\alpha}_1)\sin\gamma_{1x} \\
&\quad + \sin(2\overline{\alpha}_1)\cos\gamma_{1x}] - \eta^2 T_uF_4[\sin\gamma_{4x} \\
&\quad + \cos(2\overline{\alpha}_2)\sin\gamma_{4x} + \sin(2\overline{\alpha}_2)\cos\gamma_{4x}] \\
&\quad + \eta T_uF_2[\cos(2\overline{\alpha}_1 + 2\overline{\alpha}_2 + 2\overline{\alpha}_3)\sin\gamma_{2x} \\
&\quad - \cos(2\overline{\alpha}_3)\sin\gamma_{2x} + \sin(2\overline{\alpha}_1 \\
&\quad + 2\overline{\alpha}_2 + 2\overline{\alpha}_3)\cos\gamma_{2x} \\
&\quad + 2\sin(2\overline{\alpha}_2 + 2\overline{\alpha}_3)\cos\gamma_{2x} \\
&\quad + \sin(2\overline{\alpha}_3)\cos\gamma_{2x}] \\
\Delta T_{024} &= \overline{T}_{L2} - \overline{T}_{L4} \\
&= T_uF_1[\sin\gamma_{1x} + \cos(2\overline{\alpha}_1)\sin\gamma_{1x} \\
&\quad - \sin(2\overline{\alpha}_1)\cos\gamma_{1x}] \\
&\quad - \eta^2 T_uF_4[\sin\gamma_{4x} + \cos(2\overline{\alpha}_2)\sin\gamma_{4x} \\
&\quad - \sin(2\overline{\alpha}_2)\cos\gamma_{4x}] \\
&\quad + \eta T_uF_2[\cos(2\overline{\alpha}_3)\sin\gamma_{2x} \\
&\quad + \sin(2\overline{\alpha}_3)\cos\gamma_{2x} \\
&\quad + 2\sin(2\overline{\alpha}_2 + 2\overline{\alpha}_3)\cos\gamma \\
&\quad + \sin(2\overline{\alpha}_1 + 2\overline{\alpha}_2 + 2\overline{\alpha}_3)\cos\gamma_{2x2x} \\
&\quad - \cos(2\overline{\alpha}_1 + 2\overline{\alpha}_2 + 2\overline{\alpha}_3)\sin\gamma_{2x}] \\
\Delta T_{014} &= \overline{T}_{L1} - \overline{T}_{L4} \\
&= T_uF_1[\sin\gamma_{1x} + \cos(2\overline{\alpha}_1)\sin\gamma_{1x} \\
&\quad + \sin(2\overline{\alpha}_1)\cos\gamma_{1x}] \\
&\quad - \eta^2 T_uF_4[\sin\gamma_{4x} + \cos(2\overline{\alpha}_2)\sin\gamma_{4x} \\
&\quad - \sin(2\overline{\alpha}_2)\cos\gamma_{4x}] \\
&\quad + \eta T_uF_2[\cos(2\overline{\alpha}_2 + 2\overline{\alpha}_3)\sin\gamma_{2x} \\
&\quad \times 2\sin(2\overline{\alpha}_1 + 2\overline{\alpha}_2 + 2\overline{\alpha}_3)\cos\gamma_{2x} \\
&\quad + \sin(2\overline{\alpha}_1 + 2\overline{\alpha}_3)\cos\gamma_{2x} \\
&\quad + 2\sin(2\overline{\alpha}_2 + 2\overline{\alpha}_3)\cos\gamma_{2x} \\
&\quad - \cos(2\overline{\alpha}_2 + 2\overline{\alpha}_3)\sin\gamma_{2x}]
\end{aligned} \tag{17}$$

The dimensionless rearrangement of (17) can be written as

$$\frac{\Delta T_{012}}{T_u} = \tau_{c12}(\overline{\alpha}_1, \overline{\alpha}_2, \overline{\alpha}_3) \tag{18}$$

$$\frac{\Delta T_{023}}{T_u} - F_1 \sin\gamma_{1x} + \eta^2 F_4 \sin\gamma_{4x} = \tau_{c23}(\overline{\alpha}_1, \overline{\alpha}_2, \overline{\alpha}_3) \tag{19}$$

$$\frac{\Delta T_{034}}{T_u} = \tau_{c34}(\overline{\alpha}_1, \overline{\alpha}_2, \overline{\alpha}_3) \tag{20}$$

$$\frac{\Delta T_{013}}{T_u} - F_1 \sin\gamma_{1x} + \eta^2 F_4 \sin\gamma_{4x} = \tau_{c13}(\overline{\alpha}_1, \overline{\alpha}_2, \overline{\alpha}_3) \tag{21}$$

$$\frac{\Delta T_{024}}{T_u} - F_1 \sin\gamma_{1x} + \eta^2 F_4 \sin\gamma_{4x} = \tau_{c24}(\overline{\alpha}_1, \overline{\alpha}_2, \overline{\alpha}_3) \tag{22}$$

$$\frac{\Delta T_{014}}{T_u} - F_1 \sin\gamma_{1x} + \eta^2 F_4 \sin\gamma_{4x} = \tau_{c14}(\overline{\alpha}_1, \overline{\alpha}_2, \overline{\alpha}_3) \tag{23}$$

Here $\tau_{cij}(\overline{\alpha}_1, \overline{\alpha}_2, \overline{\alpha}_3)$ (ij = 12, 23, 34, 13, 24, 14) are the dimensionless coupling torques between motors i and j (their detailed expressions can be found in Appendix D), and are also limited functions of $\overline{\alpha}_1$, $\overline{\alpha}_2$ and $\overline{\alpha}_3$, so we have

$$|\tau_{c12}(\overline{\alpha}_1, \overline{\alpha}_2, \overline{\alpha}_3)| \le \tau_{c12max} \tag{24}$$
$$|\tau_{c23}(\overline{\alpha}_1, \overline{\alpha}_2, \overline{\alpha}_3)| \le \tau_{c23max} \tag{25}$$
$$|\tau_{c34}(\overline{\alpha}_1, \overline{\alpha}_2, \overline{\alpha}_3)| \le \tau_{c34max} \tag{26}$$
$$|\tau_{c13}(\overline{\alpha}_1, \overline{\alpha}_2, \overline{\alpha}_3)| \le \tau_{c13max} \tag{27}$$
$$|\tau_{c24}(\overline{\alpha}_1, \overline{\alpha}_2, \overline{\alpha}_3)| \le \tau_{c24max} \tag{28}$$
$$|\tau_{c14}(\overline{\alpha}_1, \overline{\alpha}_2, \overline{\alpha}_3)| \le \tau_{c14max} \tag{29}$$

Hence, the synchronization conditions of two pairs of exciters are obtained as

$$\left|\frac{\Delta T_{012}}{T_u}\right| \le \tau_{c12max} \tag{30}$$

$$\left|\frac{\Delta T_{023}}{T_u} - F_1 \sin\gamma_{1x} + \eta^2 F_4 \sin\gamma_{4x}\right| \le \tau_{c23max} \tag{31}$$

$$\left|\frac{\Delta T_{034}}{T_u}\right| \le \tau_{c34max} \tag{32}$$

$$\left|\frac{\Delta T_{013}}{T_u} - F_1 \sin\gamma_{1x} + \eta^2 F_4 \sin\gamma_{4x}\right| \le \tau_{c13max} \tag{33}$$

$$\left|\frac{\Delta T_{024}}{T_u} - F_1 \sin\gamma_{1x} + \eta^2 F_4 \sin\gamma_{4x}\right| \le \tau_{c24max} \tag{34}$$

$$\left|\frac{\Delta T_{014}}{T_u} - F_1 \sin\gamma_{1x} + \eta^2 F_4 \sin\gamma_{4x}\right| \le \tau_{c14max} \tag{35}$$

with $\Delta T_{0ij} = (T_{e0i} - f_{0i}\omega_{m0}) - (T_{e0j} - f_{0j}\omega_{m0})$.

Equations (30)∼(35) can be described as that the absolute value of dimensionless residual torque differences between arbitrary two motors are less than or equal to the maximum of their dimensionless coupling torques.

Adding all formulae of (16) up and after the rearrangement of the results of which, the average dimensionless loading torque of two pairs of motors, $\tau_a(\overline{\alpha}_1, \overline{\alpha}_2, \overline{\alpha}_3)$, can be given as

$$\begin{aligned}
&\tau_a(\overline{\alpha}_1, \overline{\alpha}_2, \overline{\alpha}_3) \\
&= \frac{1}{4T_u}\sum_{i=1}^{4}\bar{T}_{Li} \\
&= \frac{1}{2}[F_1 \sin\gamma_{1x} + F_1\cos(2\overline{\alpha}_1)\sin\gamma_{1x} \\
&\quad + \eta^2 F_4 \sin\gamma_{4x} + \eta^2 F_4 \cos(2\overline{\alpha}_2)\sin\gamma_{4x}] \\
&\quad + \frac{1}{2}\eta F_2[\cos(2\overline{\alpha}_1 + 2\overline{\alpha}_2 + 2\overline{\alpha}_3) + \cos(2\overline{\alpha}_1 + 2\overline{\alpha}_3) \\
&\quad + \cos(2\overline{\alpha}_2 + 2\overline{\alpha}_3) + \cos(2\overline{\alpha}_3)]\sin\gamma_{2x}
\end{aligned} \tag{36}$$

as such it is limited functions of $\overline{\alpha}_1$, $\overline{\alpha}_2$ and $\overline{\alpha}_3$, i.e.,

$$\tau_a(\overline{\alpha}_1, \overline{\alpha}_2, \overline{\alpha}_3) < \tau_{amax} \tag{37}$$

The coefficients of synchronization abilities between any two exciters, ξ_{ij}, therefore, are defined as

$$\zeta_{ij} = \frac{\tau_{cijmax}}{\tau_{amax}}, \quad ij = 12, 23, 34, 13, 24, 14 \tag{38}$$

The larger the coefficients ξ_{ij} are, the stronger the synchronization abilities are, and the easier the vibrating system can implement synchronization.

B. STABILITY CONDITIONS OF THE SYNCHRONOUS STATES

According to (15), one can solve several groups of the synchronous solutions on $2\alpha_i$, for these synchronous solutions, some are stable, while others are unstable, which depends on the stability condition of the system. So it is important to discuss the stability of the synchronous states of the system to determine the stable solutions as follows.

The kinetic energy (T) and potential energy (V) of the vibrating system are directly given as

$$\begin{aligned}
T &= \frac{1}{2}(M_1\dot{x}_1^2 + M_2\dot{x}_2^2 + \sum_{i=1}^{4} J_{0i}\dot{\varphi}_i^2) \\
V &= \frac{1}{2}[k_{2x}x_2^2 + k_{1x}(x_2 - x_1)^2]
\end{aligned} \tag{39}$$

Then the mean values of kinetic energy E_T and potential energy E_V over one period, can be obtained as

$$\begin{aligned}
&E_T \\
&= \frac{1}{2\pi}\int_0^{2\pi} T\,\mathrm{d}\varphi = \frac{1}{4\pi}\int_0^{2\pi}(M_1\dot{x}_1^2 + M_2\dot{x}_2^2 + \sum_{i=1}^{4} J_{0i}\dot{\varphi}_i^2)\mathrm{d}\varphi \\
&= \frac{1}{2}r^2\omega_{m0}^2\{[M_1F_1F_2\cos(\gamma_{1x} - \gamma_{2x}) \\
&\quad + M_2F_2F_4\cos(\gamma_{2x} - \gamma_{4x})]q(\overline{\alpha}_1, \overline{\alpha}_2, \overline{\alpha}_3) \\
&\quad + [M_1F_1F_2\sin(\gamma_{1x} - \gamma_{2x}) + M_2F_2F_4\sin(\gamma_{2x} - \gamma_{4x})] \\
&\quad \times p(\overline{\alpha}_1, \overline{\alpha}_2, \overline{\alpha}_3) + \left(M_1F_1^2 + M_2F_2^2\right)\left[1 + \cos(2\overline{\alpha}_1)\right] \\
&\quad + \left(M_1F_2^2 + M_2F_4^2\right)\eta^2\left[1 + \cos(2\overline{\alpha}_2)\right]\} \\
&\quad + (1 + \eta)\, m_0 r^2 \omega_{m0}^2
\end{aligned} \tag{40}$$

$$
\begin{aligned}
&E_V \\
&= \frac{1}{2\pi}\int_0^{2\pi} V\mathrm{d}\varphi = \frac{1}{4\pi}\int_0^{2\pi} [k_{2x}x_2^2 + k_{1x}(x_1 - x_2)^2]\mathrm{d}\varphi \\
&= \frac{1}{2}r^2\{[k_{1x}F_1F_2\cos(\gamma_{1x}-\gamma_{2x}) - k_{1x}F_1F_4\cos(\gamma_{1x}-\gamma_{4x}) \\
&\quad + k_{1x}F_2F_4\cos(\gamma_{2x}-\gamma_{4x}) - k_{1x}F_2^2 \\
&\quad + k_{2x}F_2F_4\cos(\gamma_{2x}-\gamma_{4x})]q(\overline{\alpha}_1,\overline{\alpha}_2,\overline{\alpha}_3) \\
&\quad + [k_{1x}F_1F_2\sin(\gamma_{1x}-\gamma_{2x}) - k_{1x}F_1F_4\sin(\gamma_{1x}-\gamma_{4x}) \\
&\quad + k_{1x}F_2F_4\sin(\gamma_{2x}-\gamma_{4x}) + k_{2x}F_2F_4\sin(\gamma_{2x}-\gamma_{4x})] \\
&\quad \times p(\overline{\alpha}_1,\overline{\alpha}_2,\overline{\alpha}_3) + [k_{1x}F_1^2 + k_{1x}F_2^2 + k_{2x}F_2^2 \\
&\quad - 2k_{1x}F_1F_2\cos(\gamma_{1x}-\gamma_{2x})][1+\cos(2\overline{\alpha}_1)] + [k_{1x}F_4^2 \\
&\quad + k_{1x}F_2^2 + k_{2x}F_4^2 - 2k_{1x}F_2F_4\cos(\gamma_{2x}-\gamma_{4x})] \\
&\quad \times \eta^2[1+\cos(2\overline{\alpha}_2)]\}
\end{aligned} \tag{41}
$$

where

$$
\begin{aligned}
q(\overline{\alpha}_1,\overline{\alpha}_2,\overline{\alpha}_3) &= \eta[\cos(2\overline{\alpha}_1 + 2\overline{\alpha}_2 + 2\overline{\alpha}_3) + \cos(2\overline{\alpha}_1 + 2\overline{\alpha}_3) \\
&\quad + \cos(2\overline{\alpha}_2 + 2\overline{\alpha}_3) + \cos(2\overline{\alpha}_3)] \\
p(\overline{\alpha}_1,\overline{\alpha}_2,\overline{\alpha}_3) &= \eta[\sin(2\overline{\alpha}_1 + 2\overline{\alpha}_2 + 2\overline{\alpha}_3) + \sin(2\overline{\alpha}_1 + 2\overline{\alpha}_3) \\
&\quad + \sin(2\overline{\alpha}_2 + 2\overline{\alpha}_3) + \sin(2\overline{\alpha}_3)]
\end{aligned}
$$

Hamilton's average action amplitude over one period, denoted by I, can be presented by

$$
I = \frac{1}{2\pi}\int_0^{2\pi}(T - V)\mathrm{d}\varphi = E_T - E_V \tag{42}
$$

Based on [12], we know that the solutions of stable phase differences (denoted by $2\overline{\alpha}_{10}$, $2\overline{\alpha}_{20}$ and $2\overline{\alpha}_{30}$) in the synchronous states correspond to the minimums of Hamilton's average action amplitudes. In other words, in order to ensure the stability of phase differences among exciters, the following Hesse matrix of I (denoted by $\mathbf{H}$) should be positive definite, where the elements of Hesse matrix of I are proposed in Appendix E.

$$
\mathbf{H} = \begin{pmatrix} d_{11} & d_{12} & d_{13} \\ d_{21} & d_{22} & d_{23} \\ d_{31} & d_{32} & d_{33} \end{pmatrix} \tag{43}
$$

The matrix $\mathbf{H}$ is positive definite, if and only if, the following conditions (44), should be satisfied.

$$
\begin{aligned}
H_1 &= d_{11} > 0 \\
H_2 &= d_{11}d_{22} - d_{12}d_{21} > 0 \\
H_3 &= d_{11}d_{22}d_{33} + d_{12}d_{23}d_{31} + d_{13}d_{21}d_{32} \\
&\quad - d_{11}d_{23}d_{32} - d_{12}d_{21}d_{33} - d_{13}d_{22}d_{31} > 0
\end{aligned} \tag{44}
$$

Equation (44), therefore, is the stability condition of the system in the synchronous states, and H_1, H_2 and H_3 are here defined as the coefficients of the stability ability.

V. NUMERICAL DYNAMIC CHARACTERISTIC DISCUSSIONS

To clearly reveal the dynamic characteristics of the system, some numerical analyses resulting from the above theoretical results are discussed in this section. The structural parameters of the system are listed in TABLE 1, based on which, the values of two critical natural frequencies, ω_2 and ω_0, are easily calculated as $\omega_2 = \sqrt{(k_{1x}+k_{2x})/M_2} \approx 74$ rad/s and $\omega_0 = \sqrt{k_{1x}/m} \approx 134$ rad/s, respectively. Additionally, here we use four identical driving motors (three-phase squirrel-cage, 50 Hz, 380 V, 0.75 kW, 6-pole, Δ-connected, and rated speed 980 r/min), and the other parameters of motors are shown in TABLE 2.

TABLE 1. Structural parameters of the system.

Contents	Values
Mass of the RF1: m_1 (kG)	600
Mass of the RF2: m_2 (kG)	1500
Mass of the standard exciter: m_0 (kG)	10
Stiffness of spring 1 in x-direction: k_{1x} (kN/m)	8000
Stiffness of spring 2 in x-direction: k_{2x} (kN/m)	100
Eccentric radius of exciters: r (m)	0.15
Critical damping ratio of relative motion between two RFs: ξ_{1x}	0.07
Critical damping ratio of the RF2: ξ_{2x}	0.07

TABLE 2. Parameters of motors.

Contents	Values
Rotor resistance: R_r (mΩ)	3400
Stator resistance: R_s (mΩ)	3350
Mutual inductance: L_m (mH)	164
Rotor inductance: L_r (mH)	170
Stator inductance: L_s (mH)	170

A. FREQUENCY-AMPLITUDE CHARACTERISTICS OF THE SYSTEM IN THE STEADY STATES

According to (9) and (11), and considering the stability conditions of the system (44), the frequency-amplitude relationships of two RFs for different η by changing the supporting frequencies in the steady state, are shown in Fig. 2, from which one can see that, the resonant regions are obviously divided into three parts (marked by Regions I, II and III) by two critical natural frequencies ω_2 and ω_0, and some characteristics are discussed in detail as following.

In Fig. 2, the practical response amplitudes of the system depend on the sum of the vibration superposition excited by two pairs of exciters, which are determined by the stable states of the phase differences among exciters for different resonant regions shown in Fig. 5. In region I of Fig. 2, the operating frequency $\omega_{m0} < \omega_2$, and the response amplitudes of two RFs are both close to zero, which implies that the exciting forces caused by exciters are not implemented positive superposition. While in region II, $\omega_2 < \omega_{m0} < \omega_0$, the operating frequency of the system is in the sub-resonant region with respect to ω_0, and the obvious resonant responses are emerged, which are results of the positive superposition

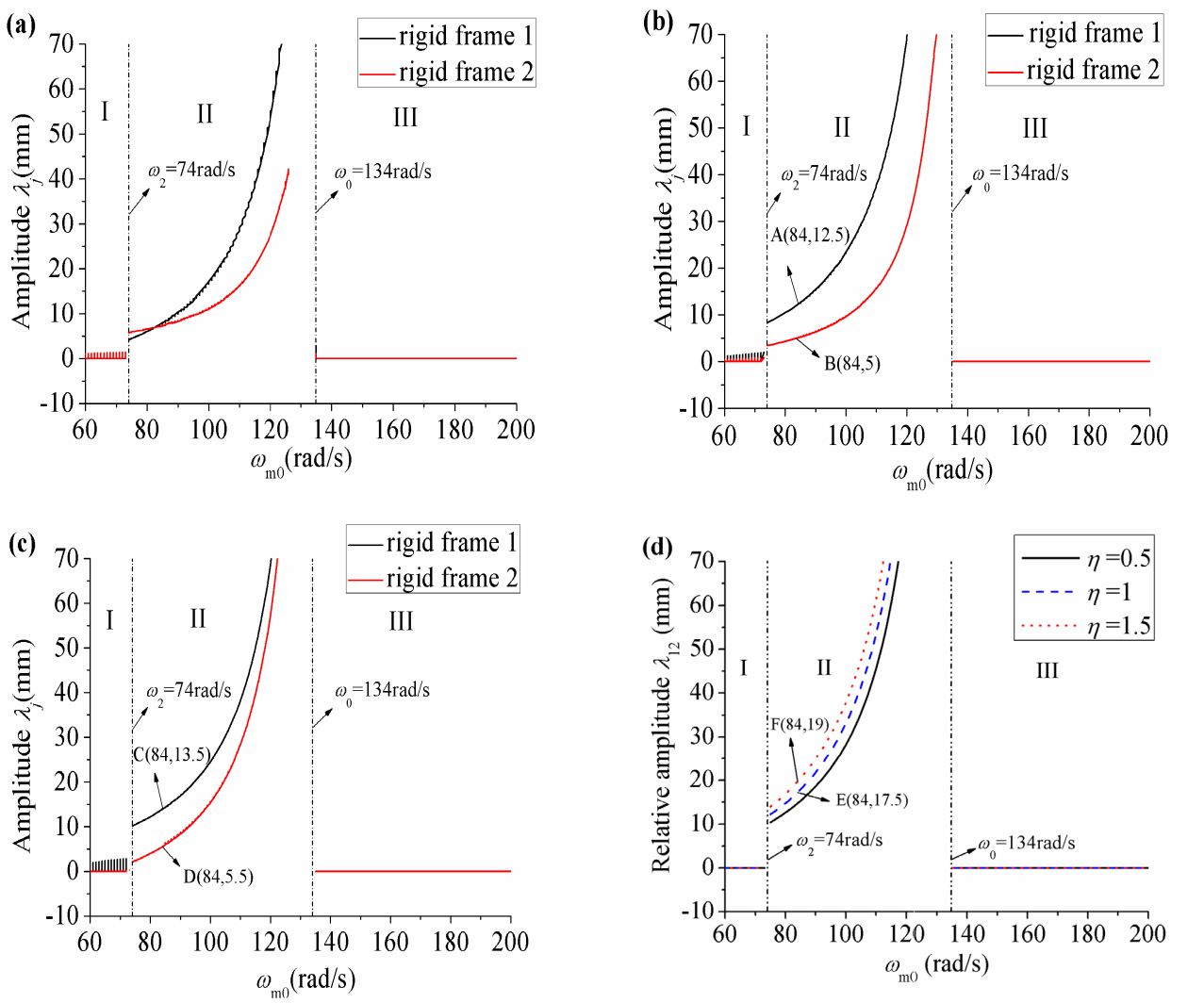

FIGURE 2. Frequency-amplitude relationships of two RFs for different values of η in the steady state: (a) $\eta = 0.5$; (b) $\eta = 1$; (c) $\eta = 1.5$; (d) frequency-amplitude relationships of the relative motion between two RFs.

of exciters, these facts can be also reflected in Region II of Fig. 5, in this case the phase difference between two exciters mounted on the same RF is equal to zero, while that on different RFs near to Pi. Additionally, in Region II of Fig. 2, the response amplitudes of two RFs are both monotonously increased with the increasing ω_{m0}, so the ideal working points of the vibrating machines should be selected in this interval in order to obtain large enough vibration amplitudes of the relative motion. In light of Region III, $\omega_{m0} > \omega_0$, the changing of frequency-amplitude curves are similar with that in region I.

It is worth noting that, the variation tendencies of different response curves are similar with each other in Fig. 2, due to the fact of the similarity of the stable phase differences among exciters shown in Fig. 5. Additionally, three curves for different η in Fig. 2(d) indicate that a larger mass ratio can provide a greater Relative Motion Response Amplitude (RMRA), so the RMRA between two RFs can be determined by adjusting the operating frequency ω_{m0} and the value of η.

From Fig. 2, it should also be seen that the frequency jump phenomenon appears at ω_2 and ω_0, this is because the stable phase differences are varied in different resonant regions, which leads to the change of the displacement response of the system.

B. COEFFICIENTS OF SYNCHRONIZATION ABILITY

Figure 3 shows the plots of coefficients of synchronization ability defined in (38) between arbitraty two exciters for different η. These coefficients are only dependent on the system structure parameters but independent on that of motors. Additionally, it can be also found that the synchronization ability is the weakest in the vicinity of ω_0, while is the strongest in the neighborhood of ω_2. In the range of $\omega_{m0} > \omega_0$, there is $\zeta_{34} < \zeta_{13} = \zeta_{23} = \zeta_{24} = \zeta_{14} < \zeta_{12}$. Furthermore, the synchronization abilities increase with the increasing η.

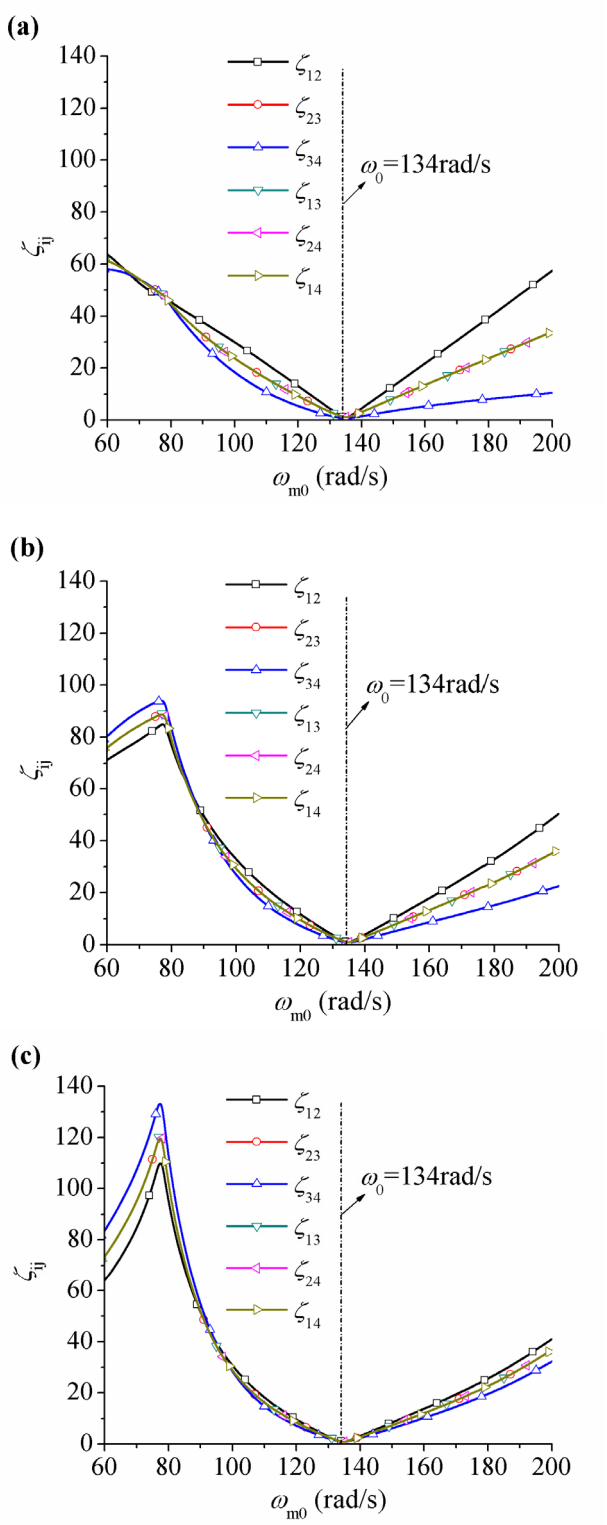

FIGURE 3. Coefficients of synchronization ability among exciters versus ω_{m0} for different η: (a) $\eta = 0.5$; (b) $\eta = 1$; (c) $\eta = 1.5$.

C. STABILITY ANALYSES OF THE SYNCHRONOUS STATES

Here the stability analyses are mainly focused on two points: the stable phase differences (SPD) among two pairs of exciters and coefficients of stability ability among them.

As it is mentioned in Section IV-B, there are many solutions corresponding to the synchronous states, some are stable, some are not stable. And the stable ones, which are discussed based on SPDs, have to be further determined by using the stability conditions (44). So the SPDs are the significant dynamic parameters to determine the final motion types of the vibrating system. Under the consideration of satisfying synchronization and stability conditions, see (17), the SPDs can be calculated by changing the value of ω_{m0}, and the plots of relationships between SPDs and ω_{m0}, are illustrated in Fig. 4. Based on the variation trends of SPDs for different η, it is clear that the plots are divided into three regions (I, II, III) by two main natural frequencies ω_0 and ω_2 (normally in engineering, $\omega_2 < \omega_0$), and these three regions cover three motion states, respectively.

On the other hand, the coefficients on stability ability of the system H_i ($i = 1, 2, 3$) can be obtained by substituting the structural parameters of the system into (44), which are shown in Fig. 5. Combined with the relationships between the SPDs and the coefficients of stability ability, some results are given as follows.

In Region I of Fig. 4 with $\omega_{m0} < \omega_2$, there are $H_1 \geq 0$, $H_2 \geq 0$ and $H_3 \geq 0$, indicating the stable operation of the system. However, the multiple groups of solutions on the SPD plots which lead the multiple equilibria of the system known as the diversity of nonlinear system [20], can be observed in Fig. 4. The stability ability is therefore weak in Region I as displayed in Fig. 5, and the stable states dependent on the initial conditions and external disturbances.

For region II of Fig. 4 with $\omega_2 < \omega_{m0} < \omega_0$, only one group of solutions on SPDs are obtained as $2\alpha_{10} = 2\alpha_{20} = 0$ and $2\alpha_{30} \approx \pm\pi$. In this case, the exciting forces excited by two exciters on the same RF implement the positive superimposition, and two RFs reflect the motion with inverse phases since $2\alpha_{30}$ is close to π. Fig. 5 indicates that the stability of the system is the strongest in this single equilibrium point state, which is exactly the desire in engineering.

For region III with $\omega_{m0} > \omega_0$, the SPDs satisfy $2\alpha_{10} = 2\alpha_{20} = \pi$, but there exist multiple solutions of $2\alpha_{30}$ in Fig. 4. In this case the exciting forces of two exciters on the same RF are compensated with each other. It follows that two RFs embody no vibration in the stead state, while the phase difference $2\alpha_{30}$ has multiple values causing the diversity of nonlinear system. Some relevant simulation analyses will be given in order to verify this property in the following sections. In addition, for the stability ability in Region III, one can see the relevant plots shown in Fig. 5.

VI. COMPUTER SIMULATIONS

In the above section, the coupling dynamic characteristics and stability of the system are studied by numeric based on the theoretical results, in which the state is divided into three resonant regions (see Regions I, II and III of Fig. 4).

In this section, further investigations will be performed by computer simulations, which are carried out by directly applying a fourth-order Runge-Kutta algorithm to (1) in order

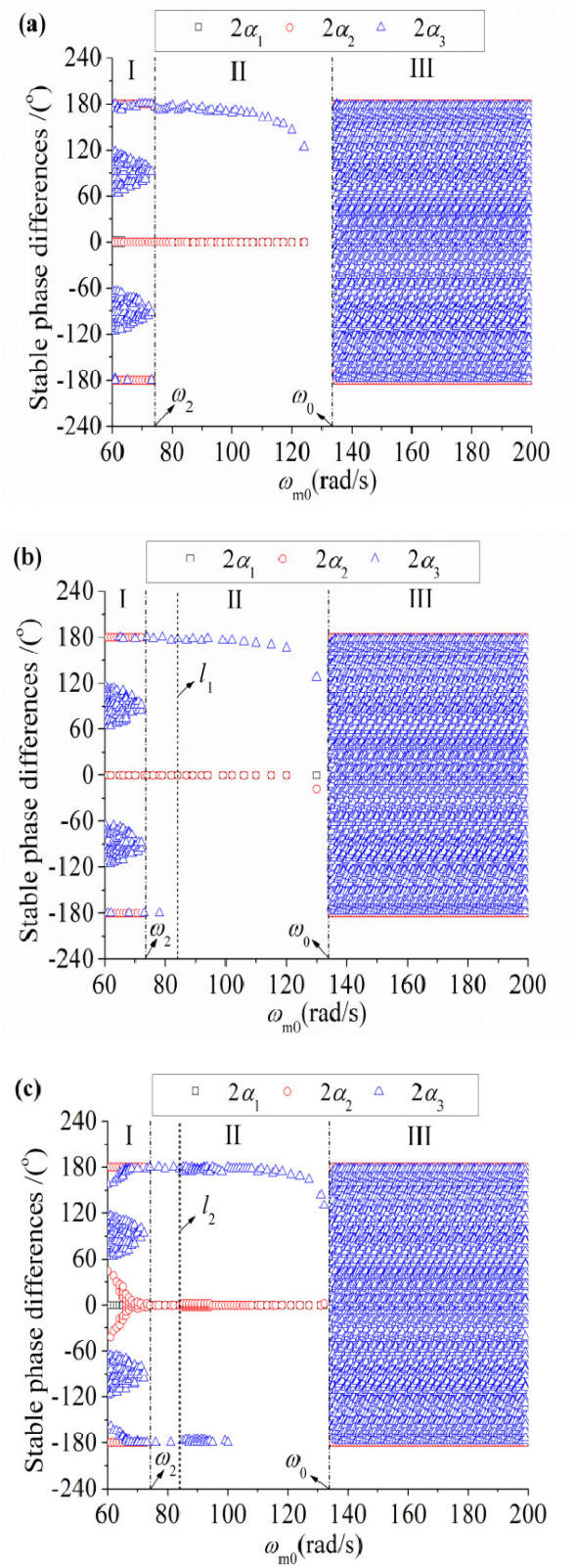

FIGURE 4. Values of stable phase differences versus ω_{m0} for different η: (a) $\eta = 0.5$; (b) $\eta = 1$; (c) $\eta = 1.5$.

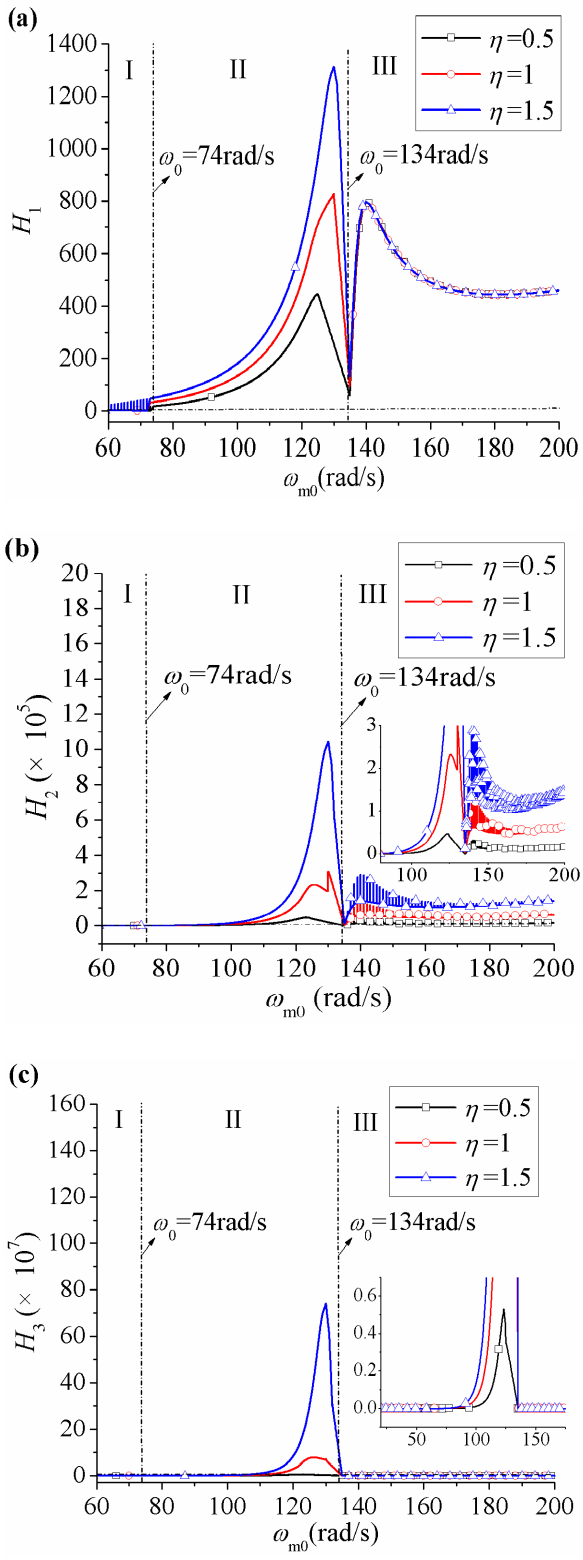

FIGURE 5. Coefficients of stability ability versus ω_{m0} for different η: (a) Values of H_1; (b) Values of H_2; (c) Value of H_3.

to verify qualitatively the theoretical and numerical results for different resonant regions (Regions I, II and III of Fig. 4) in section V. The corresponding parameters of the system are the same as those in section V except for the spring stiffness k_{1x}. Here the resonant regions of the system (i.e., the ratio between the operating frequency and natural frequency of

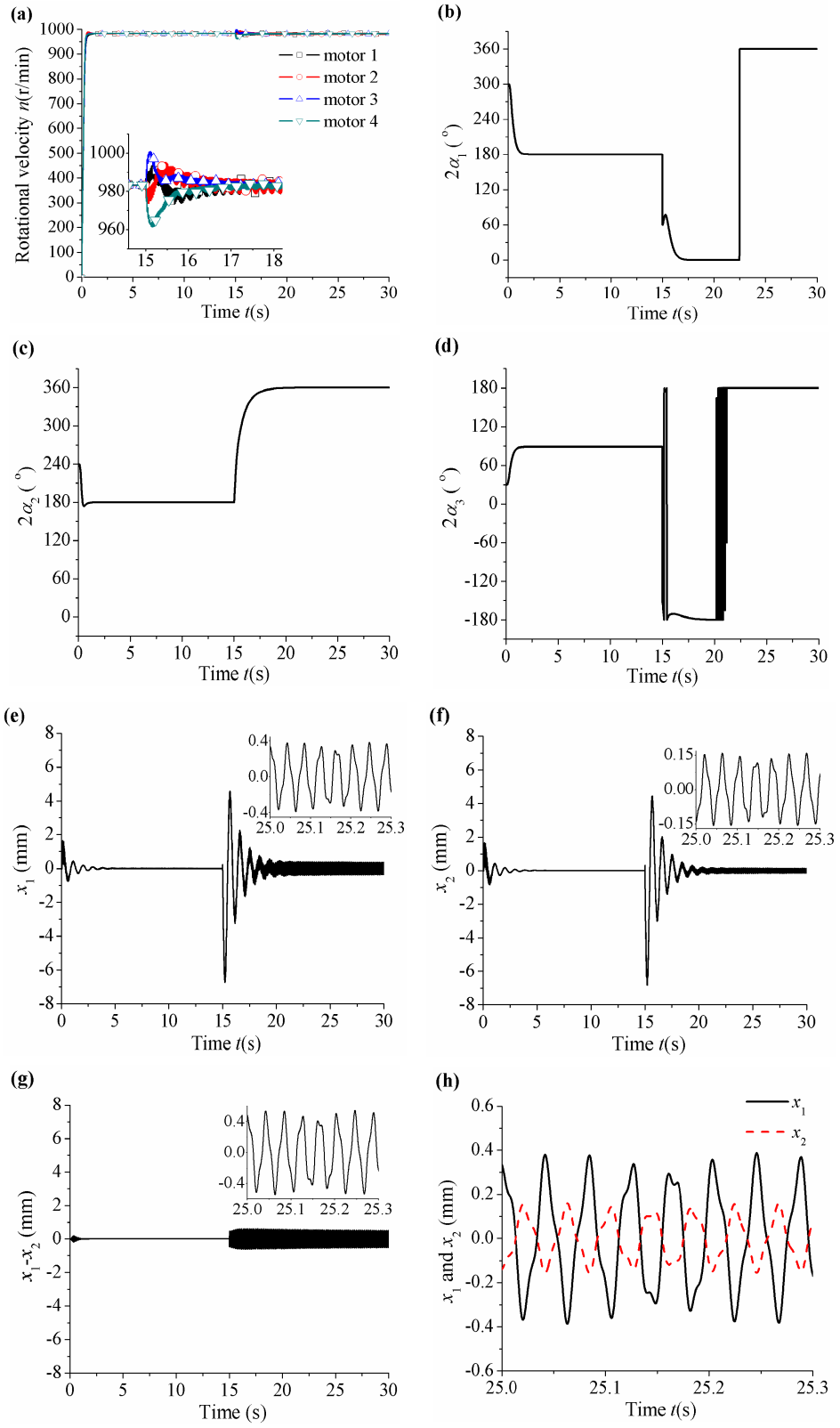

FIGURE 6. Simulation results in region I for $\eta = 1$: (a) rotational velocities of four motors; (b) phase difference between exciters 1 and 2; (c) phase difference between exciters 3 and 4; (d) phase difference between exciters 2 and 3; (e) displacement of RF1 in x-direction, (f) displacement of RF2 in x-direction; (g) relative displacement between RFs 1 and 2 in x-direction; (h) displacements of RFs 1 and 2 in x-direction.

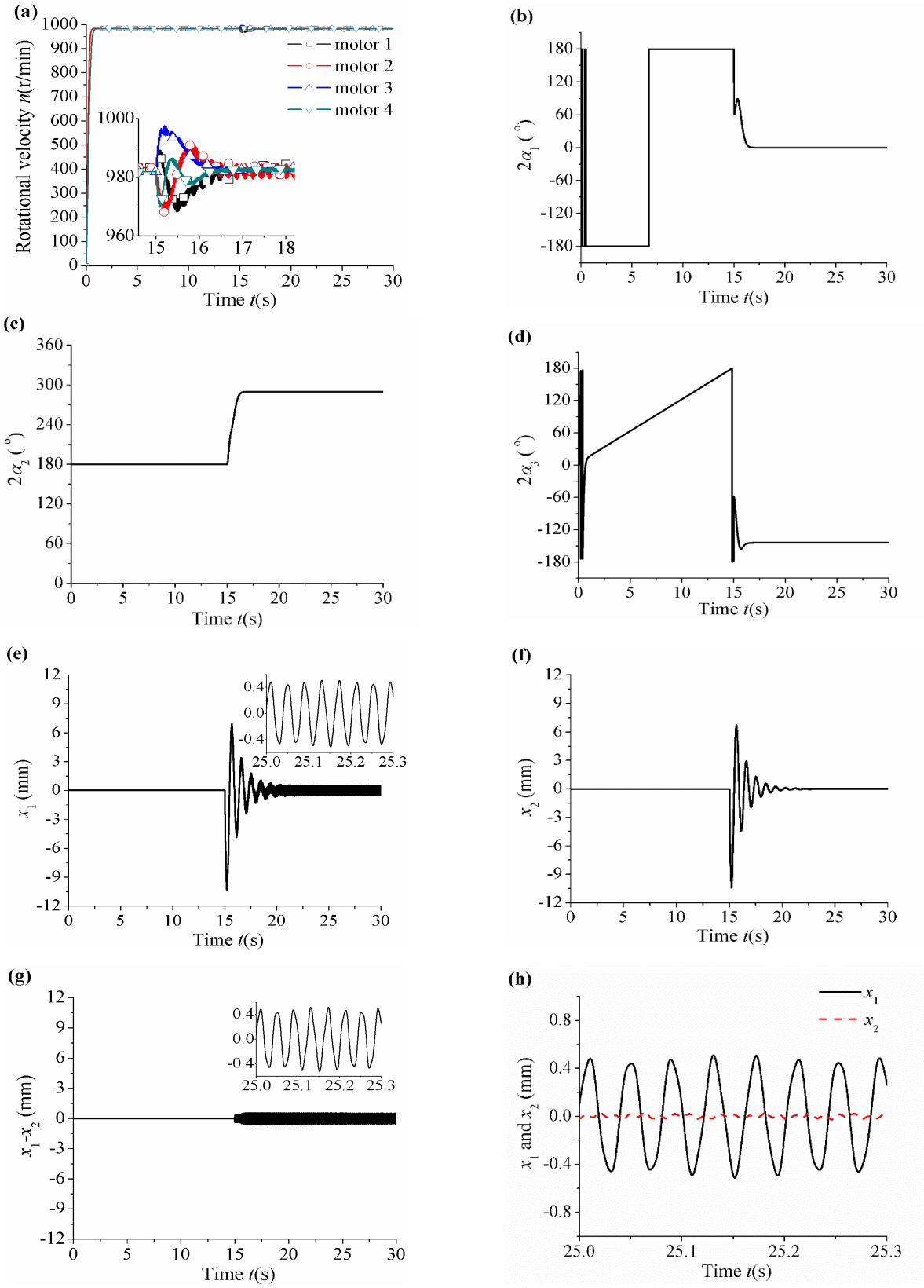

FIGURE 7. Simulation results in region I for $\eta = 1.5$: (a) rotational velocities of four motors; (b) phase difference between exciters 1 and 2; (c) phase difference between exciters 3 and 4; (d) phase difference between exciters 2 and 3; (e) displacement of RF1 in x-direction; (f) displacement of RF2 in x-direction; (g) relative displacement between RFs 1 and 2 in x-direction; (h) displacements of RFs 1 and 2 in x-direction.

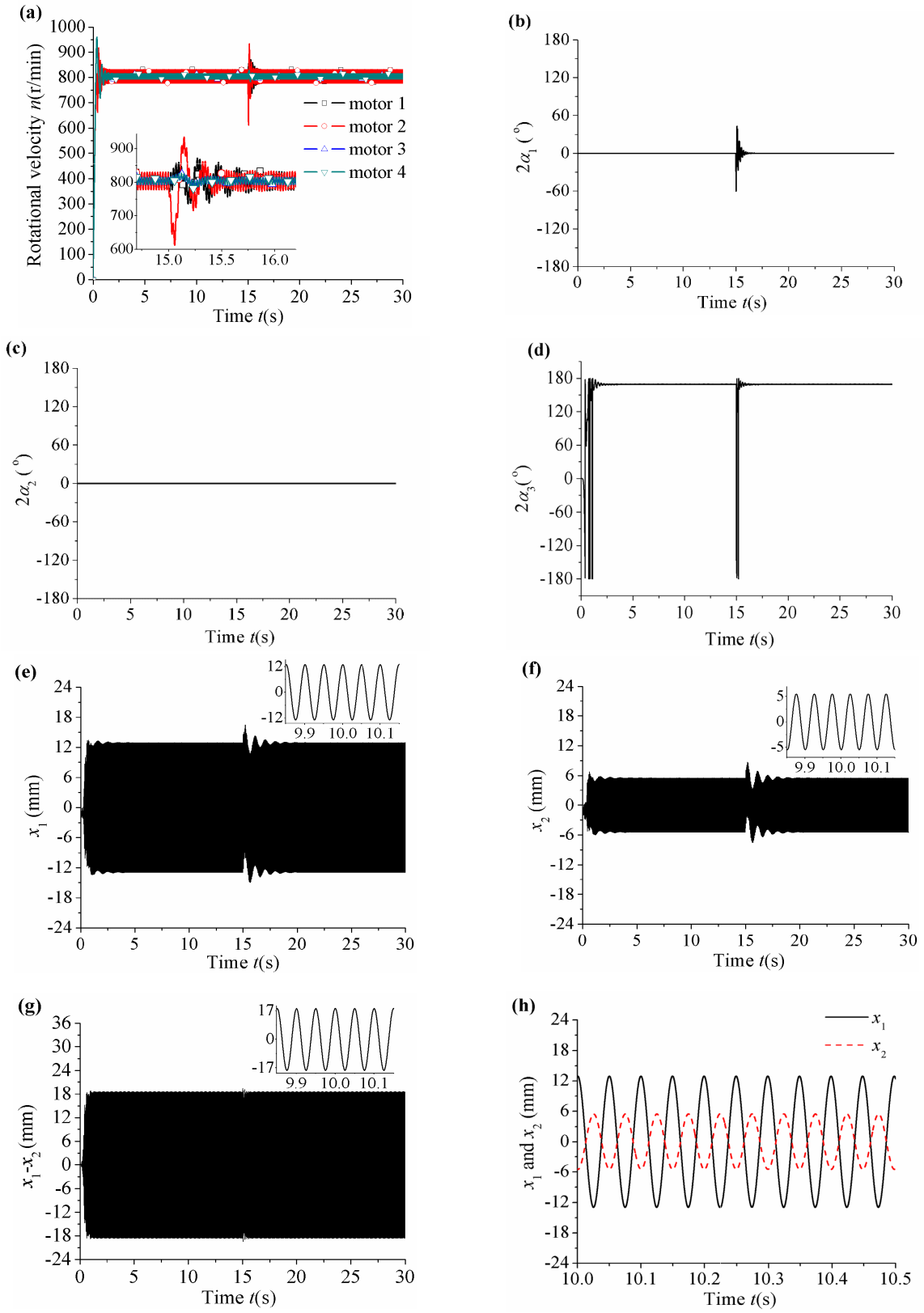

FIGURE 8. Simulation results in region II for $\eta = 1$: (a) rotational velocities of four motors; (b) phase difference between exciters 1 and 2; (c) phase difference between exciters 3 and 4; (d) phase difference between exciters 2 and 3; (e) displacement of RF1 in x-direction; (f) displacement of RF2 in x-direction; (g) relative displacement between RFs 1 and 2 in x-direction; (h) displacements of RFs 1 and 2 in x-direction.

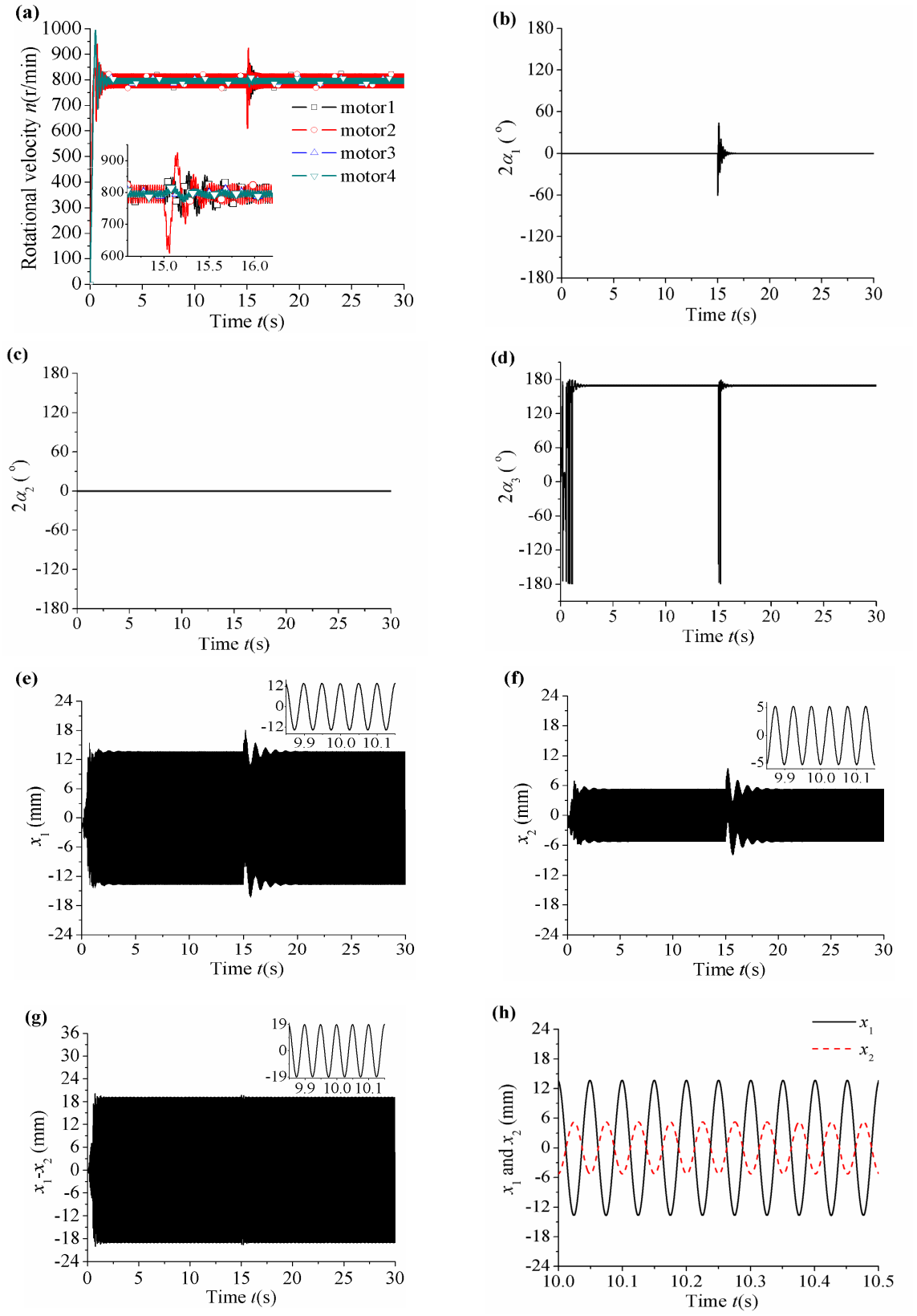

FIGURE 9. Simulation results in region II for $\eta = 1.5$: (a) rotational velocities of four motors; (b) phase difference between exciters 1 and 2; (c) phase difference between exciters 3 and 4; (d) phase difference between exciters 2 and 3; (e) displacement of RF1 in x-direction; (f) displacement of RF2 in x-direction; (g) relative displacement between RFs 1 and 2 in x-direction; (h) displacements of RFs 1 and 2 in x-direction.

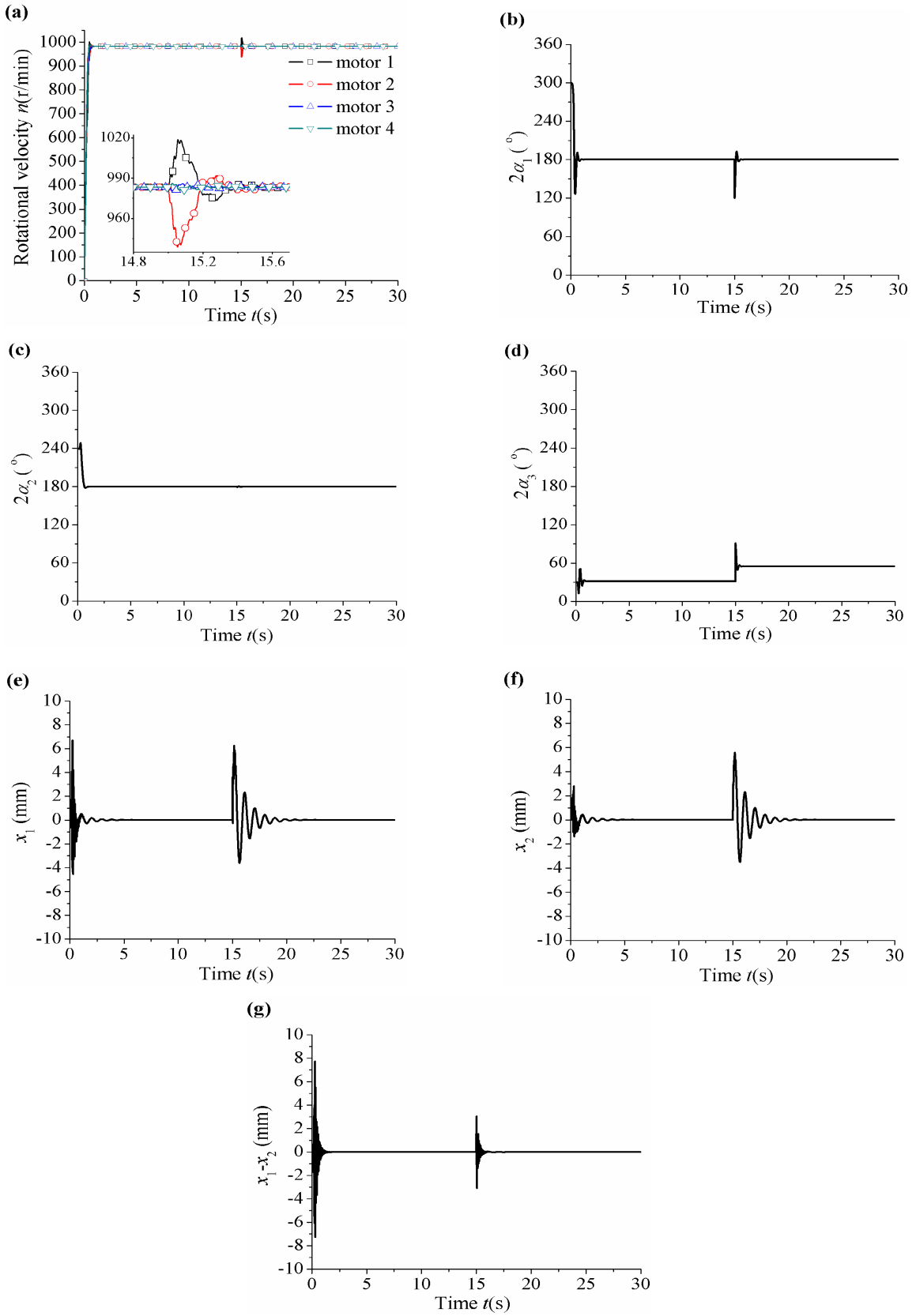

FIGURE 10. Simulation results in region III for $\eta = 1$: (a) rotational velocities of four motors; (b) phase difference between exciters 1 and 2; (c) phase difference between exciters 3 and 4; (d) phase difference between exciters 2 and 3; (e) displacement of RF1 in x-direction; (f) displacement of RF2 in x-direction; (g) relative displacement between RFs 1 and 2 in x-direction.

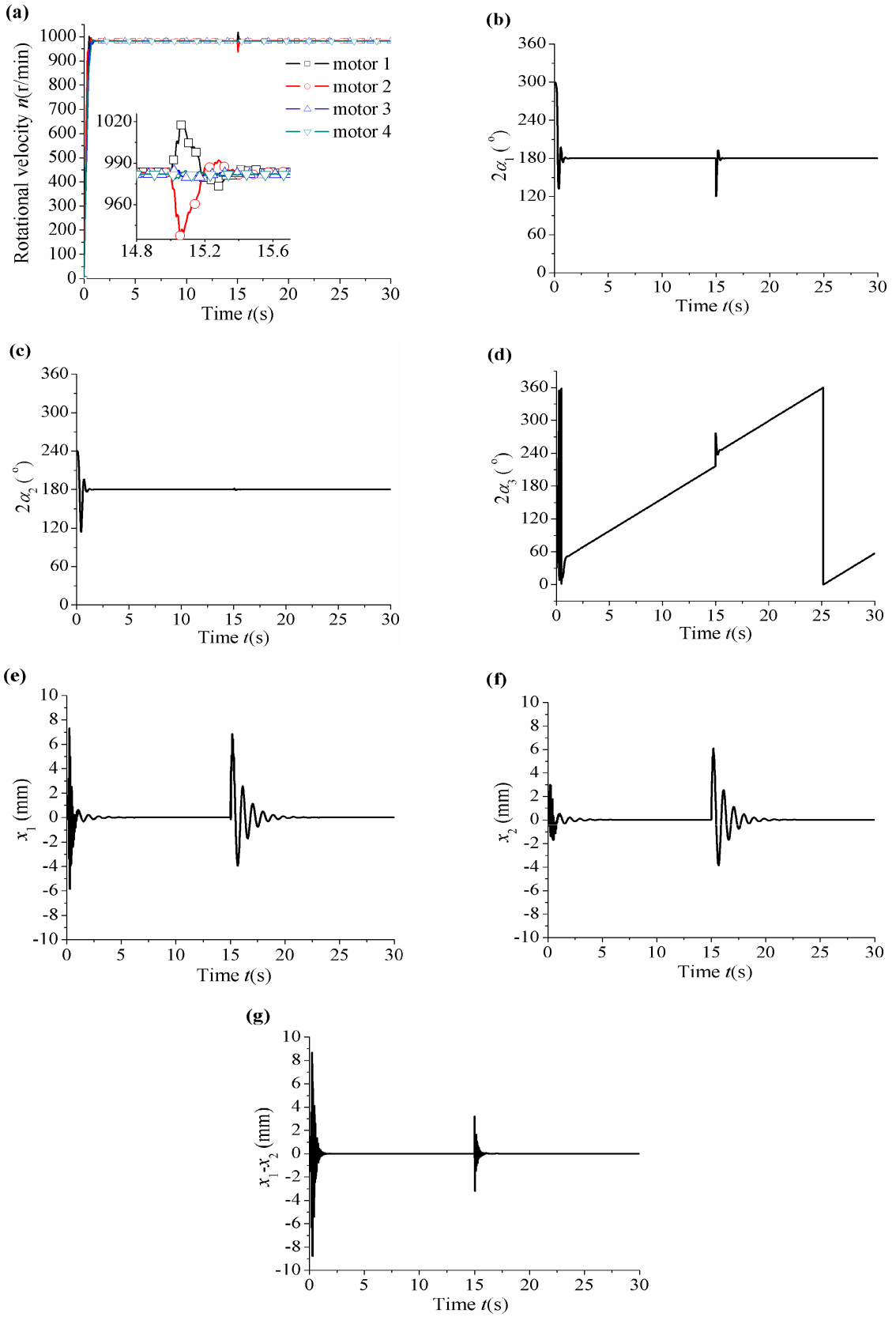

FIGURE 11. Simulation results in region III for $\eta = 1.5$: (a) rotational velocities of four motors; (b) phase difference between exciters 1 and 2; (c) phase difference between exciters 3 and 4; (d) phase difference between exciters 2 and 3; (e) displacement of RF1 in x-direction; (f) displacement of RF2 in x-direction; (g) relative displacement between RFs 1 and 2 in x-direction.

the system) are set by changing the spring stiffness k_{1x} to adjust the natural frequencies of the system. Simultaneously, two groups of simulations ($\eta = 1$ and $\eta = 1.5$) are given in each resonant region. In order to obtain the motion characteristics of the system better, the simulation time is set to 30 s in every simulation process, and the certain disturbance is added to motor 2 at 15 s.

A. SIMULATIONS OF REGION I

As shown in Figs. 6 and 7, here the spring stiffness $k_{1x} = 20000$ kN/m, and two calculated critical natural frequencies are $\omega_2 \approx 115.0$ rad/s and $\omega_0 \approx 213.2$ rad/s. See Figs. 6(a) and 7(a), the synchronously rotational velocities are all 983 r/min, i.e., the operating frequency $\omega_{m0} \approx 103$ rad/s, we have $\omega_{m0} < \omega_2$, so the system operates in Region I of Fig. 4(b)(c). The initial phases in Fig. 6 for $\eta = 1$ are set as $\varphi_1 = \pi/6$, $\varphi_2 = \pi/2$, $\varphi_3 = \pi/3$, $\varphi_4 = \pi$; while in Fig. 7 for $\eta = 1.5$, the initial phases satisfy $\varphi_1 = 0$, $\varphi_2 = \pi$, $\varphi_3 = \pi$, $\varphi_4 = 2\pi$. Additionally, when time reaches 15 s, a disturbance of phase with $2\pi/3$ is added to motor 2.

From Figs. 6 and 7, one can see that, although the rotational velocities of two pairs of exciters all reach the synchronous operation states after the first short transient process, their phase differences are not stabilized at a single equilibrium point state. As shown in Fig. 6(b)∼(d), when a disturbance of $2\pi/3$ phase is added to motor 2, $2\alpha_1$ and $2\alpha_2$ both change from 180° to 0° (or 360°), $2\alpha_3$ increases from 90° to 180°; while in Fig. 7(b)∼(d), $2\alpha_3$ reflects multiple equilibrium point states before adding a disturbance, and the phase differences between any two exciters all change from the previous stable state to another after the addition of a disturbance.

As such, the system exhibits non-harmonic responses characterized by micro-vibration, see the enlargement in Figs. 6(e)∼(h) and 7(e)∼(h). The above facts imply the characteristics of the diversity of nonlinear system [20], which all approximately agree well with what are shown in Figs. 2, 4 and 5 of section V.

B. SIMULATIONS OF REGION II

Similar with the above section VI-A, setting $k_{1x} = 8000$ kN/m, the other parameters are the same with those in section V, and the calculated critical natural frequencies: $\omega_2 \approx 74$ rad/s and $\omega_0 \approx 134$ rad/s. From Figs. 8(a) and 9(a), we can know that the synchronously rotational velocities of the system are both near 800 r/min (or $\omega_{m0} \approx 84$ rad/s), i.e., $\omega_2 < \omega_{m0} < \omega_0$, and the vibrating system can synchronously operate in resonant Region II of Fig. 4(b)(c), the corresponding simulation results are shown in the relevant plots of Figs. 8 and 9.

From Figs. 8 and 9, the initial phases of exciters all satisfy $\varphi_i = 0$ ($i = 1, 2, 3, 4$), and a phase disturbance with $\pi/3$ is added to motor 2 at 15 s. The stable phase differences of the system: $2\alpha_1 = 2\alpha_2 \approx 0°$, $2\alpha_3 \approx 168°$ in Fig. 8 for $\eta = 1$; and $2\alpha_1 = 2\alpha_2 \approx 0°$, $2\alpha_3 \approx 170°$ in Fig. 9 for $\eta = 1.5$. Although a disturbance is added to motor 2, the system still return to their previous stable states after the short adjusting process, which demonstrates the stronger stability with single equilibrium point, as shown in Figs. 8(b)∼(d) and 9(b)∼(d). What's more, the variation trends of stable phase differences in Fig. 9 are similar with those in Fig. 8, and whether the interference is added or not, the single equilibrium state of the system is not broken down. These facts are roughly coincidence with what are shown by the lines $l_1(2\alpha_1 = 2\alpha_2 \approx 0°, 2\alpha_3 \approx 168.5°)$ and $l_2(2\alpha_1 = 2\alpha_2 \approx 0°, 2\alpha_3 \approx 171°)$ in Fig. 4(b) and 4(c), respectively.

Seeing the displacements of two RFs for the case of $\eta = 1$ shown in Fig. 8(e)∼(g), the vibration amplitudes of RF1 and RF2 are about 12.5 mm and 5 mm, respectively, and the relative displacement between two RFs is close to 17.5 mm in Fig. 8(g), which are in good agreement with the points A, B and E in Fig. 2. As such, for the case of $\eta = 1.5$ shown in Fig. 9(e)∼(g), which is similar with that in Fig. 8, and here no further discussions. It should be mentioned that the motion types between two RFs are obviously inverse phases, as shown in the enlargement of Figs. 8(h) and 9(h), which verifies indirectly the physical property of ω_0 given in sections V-A, i.e., it is referred to be as the natural frequency of the relative motion with inverse phases between two RFs.

C. SIMULATIONS OF REGION III

In this section setting $k_{1x} = 3000$ kN/m, the simulations of Region III for different mass ratios of exciters can be seen in Figs. 10 and 11, where two natural frequencies are solved as $\omega_2 \approx 45.2$ rad/s and $\omega_0 \approx 82.5$ rad/s. From Figs. 10(a) and 11(a), the synchronously rotational velocities of the system are both stabilized at 983 r/min (or $\omega_{m0} \approx 103$ rad/s), we have $\omega_{m0} > \omega_0$, and the system can synchronously operate in Region III of Fig. 4(b)(c). Similar to what are illustrated in Fig. 6, the initial phases satisfy $\varphi_1 = \pi/6$, $\varphi_2 = \pi/2$, $\varphi_3 = \pi/3$, $\varphi_4 = \pi$, and a disturbance of $\pi/3$ phase is added to the motor 2 at 15s.

In Figs. 10 and 11, when a disturbance is added to the motor 2, the simulation results in region III are similar with those in region I, i.e., $2\alpha_1$ and $2\alpha_2$ have no change of the equilibrium state in Figs. 10 and 11. However, $2\alpha_3$ changes from 31° to 55° in Fig. 10(d), and $2\alpha_3$ in Fig. 11(d) always keeps unstable no matter whether a disturbance is added. These facts verify the phenomenon of the diversity of nonlinear system shown in Fig. 4.

Additionally, according to the values of stable phase differences, it can be noted that the exciting forces acting on two RFs are cancelled mutually, see Figs. 10 and 11, so the motion type of two RFs is no vibration in the steady state. These results can roughly agree with what are shown in Fig. 2.

VII. CONCLUSION

This paper proposes an analytical approach to investigate stability of the synchronous states of two pairs of exciters distributed on different RFs. The criterions of implementing synchronization and stability are obtained theoretically, and the coupling characteristics of the system are discussed by numeric, in which the resonant region of the system is divided

into three parts: (I) $\omega_{m0} < \omega_2$; (II) $\omega_2 < \omega_{m0} < \omega_0$; (III) $\omega_{m0} > \omega_0$, based on the ratios of the operation frequency ω_{m0} to natural frequencies (ω_2 and ω_0).

According to the results of dynamic analyses and simulations, the motion types of two RFs in Regions I and III are similar with each other in the steady state, in this case the diversity of nonlinear system is appeared, which kind of equilibrium state to be occurred is dependent on the initial conditions and external disturbances, and the displacements of two RFs are both close to zero, the motion type of the system reflects no vibration. However, in region II the phase differences of each pair of exciters on the same RFs are all stabilized in the vicinity of zero, the corresponding exciting forces are superimposed positively, while the phase differences between two exciters on different RFs are stabilized in the neighborhood of π, and two RFs realize the relative motion with inverse phases, which is the desire in engineering.

By the comparisons of theory, numerical characteristic analyses and simulations, the theoretical method used is proved to be feasible and valid. The ideal working points of such kinds of vibrating machines used in engineering, should be selected in region II with $\omega_2 < \omega_{m0} < \omega_0$. Only in this way, can the stronger relative vibration amplitude with inverse phases between two RFs be obtained.

The present work can be as a theoretical reference for designing some new vibrating equipments, such as vibrating shock crushers, vibrating activate feeder, and so on.

APPENDIX A
COEFFICIENTS OF EQ. (10)

$$F_1 = m_0\omega_{m0}^2\sqrt{\frac{c^2+d^2}{a^2+b^2}}, \quad F_2 = F_3 = m_0\omega_{m0}^2\sqrt{\frac{e^2+f^2}{a^2+b^2}},$$

$$F_4 = m_0\omega_{m0}^2\sqrt{\frac{g^2+f^2}{a^2+b^2}},$$

$$\gamma_{1x} = \begin{cases} \arctan\dfrac{bc-ad}{ac+bd}, & ac+bd > 0 \\ \pi + \arctan\dfrac{bc-ad}{ac+bd}, & ac+bd < 0, \end{cases}$$

$$\gamma_{2x} = \gamma_{3x} = \begin{cases} \arctan\dfrac{be-af}{ae+bf}, & ae+bf > 0 \\ \pi + \arctan\dfrac{be-af}{ae+bf}, & ae+bf < 0, \end{cases}$$

$$\gamma_{4x} = \begin{cases} \arctan\dfrac{bg-af}{ag+bf}, & ag+bf > 0 \\ \pi + \arctan\dfrac{bg-af}{ag+bf}, & ag+bf < 0, \end{cases}$$

$$\begin{aligned} a &= M_1M_2\omega_{m0}^4 - (M_1k_{1x} + M_2k_{1x} \\ &\quad + M_1k_{2x} + f_{1x}f_{2x})\omega_{m0}^2 + k_{1x}k_{2x}, \\ b &= -(M_1f_{1x} + M_2f_{1x} + M_1f_{2x})\omega_{m0}^3 + (k_{1x}f_{2x} + k_{2x}f_{1x})\omega_{m0}, \\ c &= -M_2\omega_{m0}^2 + k_{1x} + k_{2x}, \quad d = (f_{1x} + f_{2x})\omega_{m0}, \ e = k_{1x}, \\ f &= f_{1x}\omega_{m0}, \ g = -M_1\omega_{m0}^2 + k_{1x}. \end{aligned}$$

APPENDIX B
PARAMETERS OF EQ. (11)

$$\begin{aligned} A_1 &= F_1r[\cos(\nu_1 - \gamma_{1x}) + \cos(\nu_2 - \gamma_{1x})] \\ &\quad + \eta F_3r[\cos(\nu_1 - \gamma_{1x}) + \cos(\nu_2 - \gamma_{1x})] \\ B_1 &= F_1r[\sin(\nu_1 - \gamma_{1x}) + \sin(\nu_2 - \gamma_{1x})] \\ &\quad + \eta F_3r[\sin(\nu_1 - \gamma_{1x}) + \sin(\nu_2 - \gamma_{1x})] \\ C_1 &= F_2r[\cos(\nu_1 - \gamma_{1x}) + \cos(\nu_2 - \gamma_{1x})] \\ &\quad + \eta F_4r[\cos(\nu_1 - \gamma_{1x}) + \cos(\nu_2 - \gamma_{1x})] \\ D_1 &= F_2r[\sin(\nu_1 - \gamma_{1x}) + \sin(\nu_2 - \gamma_{1x})] \\ &\quad + \eta F_4r[\sin(\nu_1 - \gamma_{1x}) + \sin(\nu_2 - \gamma_{1x})] \end{aligned}$$

APPENDIX C
COEFFICIENTS OF EQ. (16)

$$\begin{aligned} &F_1 \\ &= m_0\omega_{m0}^2\sqrt{\frac{c^2+d^2}{a^2+b^2}} \\ &= \sqrt{\frac{r_{m1}^2\left(\frac{1}{z_2^2}-1\right)^2 + f_1(\xi_{1x},\xi_{2x})}{\left(1-\frac{1}{z_{inv}^2}\right)^2\left(1-\frac{1}{z_{sa}^2}\right)^2 + f_3(\xi_{1x},\xi_{2x}) + f_4(\xi_{1x},\xi_{2x})}}, \\ &F_2 \\ &= F_3 = m_0\omega_{m0}^2\sqrt{\frac{e^2+f^2}{a^2+b^2}} \\ &= \sqrt{\frac{\frac{r_m^2}{z_0^4} + f_2(\xi_{1x},\xi_{2x})}{\left(1-\frac{1}{z_{inv}^2}\right)^2\left(1-\frac{1}{z_{sa}^2}\right)^2 + f_3(\xi_{1x},\xi_{2x}) + f_4(\xi_{1x},\xi_{2x})}}, \\ &F_4 \\ &= m_0\omega_{m0}^2\sqrt{\frac{f^2+g^2}{a^2+b^2}} \\ &= \sqrt{\frac{r_{m2}^2\left(\frac{1}{z_1^2}-1\right)^2 + f_2(\xi_{1x},\xi_{2x})}{\left(1-\frac{1}{z_{inv}^2}\right)^2\left(1-\frac{1}{z_{sa}^2}\right)^2 + f_3(\xi_{1x},\xi_{2x}) + f_4(\xi_{1x},\xi_{2x})}}, \\ &r_m \\ &= \frac{m_0}{M}, \ r_{m1} = \frac{m_0}{M_1}, \ r_{m2} = \frac{m_0}{M_2}, \ \omega_0 = \sqrt{\frac{k_{1x}}{m}}, \ \omega_1 = \sqrt{\frac{k_{1x}}{M_1}}, \\ &\omega_2 \\ &= \sqrt{\frac{k_{1x}+k_{2x}}{M_2}}, \quad \omega_g = \sqrt{\frac{k_{2x}}{M}}, \ z_{inv} = \frac{\omega_{m0}}{\omega'_{inv}}, \ z_{sa} = \frac{\omega_{m0}}{\omega'_{sa}}, \\ &z_0 \\ &= \frac{\omega_{m0}}{\omega_0}, \quad z_1 = \frac{\omega_{m0}}{\omega_1}, \ z_2 = \frac{\omega_{m0}}{\omega_2}, \ z_g = \frac{\omega_{m0}}{\omega_g}, \\ &\xi_{1x} \\ &= \frac{f_{1x}}{2\sqrt{k_{1x}M}}, \quad \xi_{2x} = \frac{f_{2x}}{2\sqrt{k_{2x}M}}, \\ &f_1(\xi_{1x},\xi_{2x}) \\ &= 4\left(\frac{r_m\xi_{1x}}{z_0} + \frac{r_{m1}r_{m2}\xi_{2x}}{r_m z_g}\right)^2, \quad f_2(\xi_{1x},\xi_{2x}) = \frac{4r_m^2\xi_{2x}^2}{z_0^2}, \end{aligned}$$

$$f_3(\xi_{1x},\xi_{2x}) = \frac{8\xi_{1x}\xi_{2x}}{z_0^2 z_g}[\frac{2\xi_{1x}\xi_{2x}}{z_g} - z_0\left(1-\frac{1}{z_{inv}^2}\right)\left(1-\frac{1}{z_{sa}^2}\right)],$$

$$f_4(\xi_{1x},\xi_{2x}) = \frac{4}{z_0^4}\left[\frac{1}{z_g}\left(\xi_{2x} - \frac{r_{m2}\xi_{2x}z_0^2}{r_m} + \frac{\xi_{1x}z_0}{z_g}\right) - z_0\xi_{1x}\right]^2.$$

APPENDIX D
COEFFICIENTS OF EQS. (18)-(23)

$$\begin{aligned}
&\tau_{c12}(\overline{\alpha}_1,\overline{\alpha}_2,\overline{\alpha}_3)\\
&= 2F_1\sin(2\overline{\alpha}_1)\cos\gamma_{1x} + \eta F_2[\cos(2\overline{\alpha}_1\\
&\quad + 2\overline{\alpha}_2 + 2\overline{\alpha}_3)\sin\gamma_{2x} + \cos(2\overline{\alpha}_1 + 2\overline{\alpha}_3)\sin\gamma_{2x}\\
&\quad - \cos(2\overline{\alpha}_2 + 2\overline{\alpha}_3)\sin\gamma_{2x} - \cos(2\overline{\alpha}_3)\sin\gamma_{2x}\\
&\quad + \sin(2\overline{\alpha}_1 + 2\overline{\alpha}_2 + 2\overline{\alpha}_3)\cos\gamma_{2x} - \sin(2\overline{\alpha}_3)\cos\gamma_{2x}\\
&\quad + \sin(2\overline{\alpha}_1 + 2\overline{\alpha}_3)\cos\gamma_{2x} - \sin(2\overline{\alpha}_2 + 2\overline{\alpha}_3)\cos\gamma_{2x}]\\
&\tau_{c23}(\overline{\alpha}_1,\overline{\alpha}_2,\overline{\alpha}_3)\\
&= F_1[\cos(2\overline{\alpha}_1)\sin\gamma_{1x} - \sin(2\overline{\alpha}_1)\cos\gamma_{1x}]\\
&\quad - \eta^2 F_4[\cos(2\overline{\alpha}_2)\sin\gamma_{4x} + \sin(2\overline{\alpha}_2)\cos\gamma_{4x}]\\
&\quad + \eta F_2[\cos(2\overline{\alpha}_2 + 2\overline{\alpha}_3)\sin\gamma_{2x} - \cos(2\overline{\alpha}_1 + 2\overline{\alpha}_3)\sin\gamma_{2x}\\
&\quad + \sin(2\overline{\alpha}_1 + 2\overline{\alpha}_3)\cos\gamma_{2x}\\
&\quad - \sin(2\overline{\alpha}_2 + 2\overline{\alpha}_3)\cos\gamma_{2x}\\
&\quad + 2\sin(2\overline{\alpha}_3)\cos\gamma_{2x}]\\
&\tau_{c12}(\overline{\alpha}_1,\overline{\alpha}_2,\overline{\alpha}_3)\\
&= 2\eta^2 F_4\sin(2\overline{\alpha}_2)\cos\gamma_{4x}\\
&\quad + \eta F_2[\cos(2\overline{\alpha}_1 + 2\overline{\alpha}_3)\sin\gamma_{2x} + \cos(2\overline{\alpha}_3)\sin\gamma_{2x}\\
&\quad - \cos(2\overline{\alpha}_1 + 2\overline{\alpha}_2 + 2\overline{\alpha}_3)\sin\gamma_{2x}\\
&\quad - \cos(2\overline{\alpha}_2 + 2\overline{\alpha}_3)\sin\gamma_{2x}\\
&\quad + \sin(2\overline{\alpha}_1 + 2\overline{\alpha}_2 + 2\overline{\alpha}_3)\cos\gamma_{2x} - \sin(2\overline{\alpha}_3)\cos\gamma_{2x}\\
&\quad + \sin(2\overline{\alpha}_1 + 2\overline{\alpha}_3)\cos\gamma_{2x}\\
&\quad - \sin(2\overline{\alpha}_2 + 2\overline{\alpha}_3)\cos\gamma_{2x}]\\
&\tau_{c13}(\overline{\alpha}_1,\overline{\alpha}_2,\overline{\alpha}_3)\\
&= F_1[\cos(2\overline{\alpha}_1)\sin\gamma_{1x}\\
&\quad + \sin(2\overline{\alpha}_1)\cos\gamma_{1x}]\\
&\quad - \eta^2 F_4[\cos(2\overline{\alpha}_2)\sin\gamma_{4x} + \sin(2\overline{\alpha}_2)\cos\gamma_{4x}]\\
&\quad + \eta F_2[\cos(2\overline{\alpha}_1 + 2\overline{\alpha}_2 + 2\overline{\alpha}_3)\sin\gamma_{2x}\\
&\quad - \cos(2\overline{\alpha}_3)\sin\gamma_{2x} + \sin(2\overline{\alpha}_1 + 2\overline{\alpha}_2 + 2\overline{\alpha}_3)\cos\gamma_{2x}\\
&\quad + 2\sin(2\overline{\alpha}_1 + 2\overline{\alpha}_3)\cos\gamma_{2x} + \sin(2\overline{\alpha}_3)\cos\gamma_{2x}]\\
&\tau_{c24}(\overline{\alpha}_1,\overline{\alpha}_2,\overline{\alpha}_3)\\
&= F_1[\cos(2\overline{\alpha}_1)\sin\gamma_{1x}\\
&\quad - \sin(2\overline{\alpha}_1)\cos\gamma_{1x}]\\
&\quad - \eta^2 F_4[\cos(2\overline{\alpha}_2)\sin\gamma_{4x} - \sin(2\overline{\alpha}_2)\cos\gamma_{4x}]\\
&\quad + \eta F_2[\cos(2\overline{\alpha}_3)\sin\gamma_{2x} - \cos(2\overline{\alpha}_1 + 2\overline{\alpha}_2\\
&\quad + 2\overline{\alpha}_3)\sin\gamma_{2x} + \sin(2\overline{\alpha}_1 + 2\overline{\alpha}_2 + 2\overline{\alpha}_3)\cos\gamma_{2x}\\
&\quad + 2\sin(2\overline{\alpha}_2 + 2\overline{\alpha}_3)\cos\gamma_{2x} + \sin(2\overline{\alpha}_3)\cos\gamma_{2x}]\\
&\tau_{c14}(\overline{\alpha}_1,\overline{\alpha}_2,\overline{\alpha}_3)\\
&= F_1[\cos(2\overline{\alpha}_1)\sin\gamma_{1x}\\
&\quad + \sin(2\overline{\alpha}_1)\cos\gamma_{1x}] - \eta^2 F_4[\cos(2\overline{\alpha}_2)\sin\gamma_{4x}\\
&\quad - \sin(2\overline{\alpha}_2)\cos\gamma_{4x}] + \eta F_2[\cos(2\overline{\alpha}_1 + 2\overline{\alpha}_3)\sin\gamma_{2x}\\
&\quad - \cos(2\overline{\alpha}_2 + 2\overline{\alpha}_3)\sin\gamma_{2x} + \sin(2\overline{\alpha}_1 + 2\overline{\alpha}_3)\cos\gamma_{2x}\\
&\quad + \sin(2\overline{\alpha}_2 + 2\overline{\alpha}_3)\cos\gamma_{2x} + 2\sin(2\overline{\alpha}_1\\
&\quad + 2\overline{\alpha}_2 + 2\overline{\alpha}_3)\cos\gamma_{2x}]
\end{aligned}$$

APPENDIX E
ELEMENTS OF THE MATRIX H OF EQ. (43)

$$\begin{aligned}
d_{11} &= \frac{\partial^2 I}{\partial\overline{\alpha}_1^2}\\
&= Q\eta[\cos(2\overline{\alpha}_{10} + 2\overline{\alpha}_{20} + 2\overline{\alpha}_{30}) + \cos(2\overline{\alpha}_{10} + 2\overline{\alpha}_{30})]\\
&\quad + P\eta[\sin(2\overline{\alpha}_{10} + 2\overline{\alpha}_{20} + 2\overline{\alpha}_{30}) + \sin(2\overline{\alpha}_{10} + 2\overline{\alpha}_{30})]\\
&\quad - 2r^2\omega_{m0}^2(M_1F_1^2 + M_2F_2^2)\cos(2\overline{\alpha}_{10})\\
&\quad + 2r^2[k_{1x}F_1^2 + k_{1x}F_2^2\\
&\quad + k_{2x}F_2^2 - 2k_{1x}F_1F_2\cos(\gamma_{1x} - \gamma_{2x})]\cos(2\overline{\alpha}_{10})\\
d_{12} &= d_{21} = \frac{\partial^2 I}{\partial\overline{\alpha}_1\partial\overline{\alpha}_2}\\
&= Q\eta\cos(2\overline{\alpha}_{10} + 2\overline{\alpha}_{20} + 2\overline{\alpha}_{30})\\
&\quad + P\eta\sin(2\overline{\alpha}_{10} + 2\overline{\alpha}_{20} + 2\overline{\alpha}_{30})\\
d_{13} &= d_{31} = \frac{\partial^2 I}{\partial\overline{\alpha}_1\partial\overline{\alpha}_3}\\
&= Q\eta[\cos(2\overline{\alpha}_{10} + 2\overline{\alpha}_{20} + 2\overline{\alpha}_{30}) + \cos(2\overline{\alpha}_{10} + 2\overline{\alpha}_{30})]\\
&\quad + P\eta[\sin(2\overline{\alpha}_{10} + 2\overline{\alpha}_{20} + 2\overline{\alpha}_{30}) + \sin(2\overline{\alpha}_{10} + 2\overline{\alpha}_{30})]\\
d_{22} &= \frac{\partial^2 I}{\partial\overline{\alpha}_2^2}\\
&= Q\eta[\cos(2\overline{\alpha}_{10} + 2\overline{\alpha}_{20} + 2\overline{\alpha}_{30})\\
&\quad + \cos(2\overline{\alpha}_{20} + 2\overline{\alpha}_{30})] + P\eta[\sin(2\overline{\alpha}_{10}\\
&\quad + 2\overline{\alpha}_{20} + 2\overline{\alpha}_{30}) + \sin(2\overline{\alpha}_{20} + 2\overline{\alpha}_{30})]\\
&\quad - 2r^2\omega_{m0}^2(M_1F_2^2 + M_2F_4^2)\eta^2\cos(2\overline{\alpha}_{20})\\
&\quad + 2r^2[k_{1x}F_4^2 + k_{1x}F_2^2 + k_{2x}F_4^2\\
&\quad - 2k_{1x}F_2F_4\cos(\gamma_{2x} - \gamma_{4x})]\eta^2\cos(2\overline{\alpha}_{20})\\
d_{23} &= d_{32} = \frac{\partial^2 In}{\partial\overline{\alpha}_2\partial\overline{\alpha}_3}\\
&= Q\eta[\cos(2\overline{\alpha}_{10} + 2\overline{\alpha}_{20} + 2\overline{\alpha}_{30})\\
&\quad + \cos(2\overline{\alpha}_{20} + 2\overline{\alpha}_{30})] + P\eta[\sin(2\overline{\alpha}_{10}\\
&\quad + 2\overline{\alpha}_{20} + 2\overline{\alpha}_{30}) + \sin(2\overline{\alpha}_{20} + 2\overline{\alpha}_{30})]\\
d_{33} &= \frac{\partial^2 In}{\partial\overline{\alpha}_3^2}\\
&= Q\eta[\cos(2\overline{\alpha}_{10} + 2\overline{\alpha}_{20} + 2\overline{\alpha}_{30})\\
&\quad + \cos(2\overline{\alpha}_{10} + 2\overline{\alpha}_{30})\\
&\quad + \cos(2\overline{\alpha}_{20} + 2\overline{\alpha}_{30}) + \cos(2\overline{\alpha}_{30})]\\
&\quad + P\eta[\sin(2\overline{\alpha}_{10} + 2\overline{\alpha}_{20} + 2\overline{\alpha}_{30}) + \sin(2\overline{\alpha}_{10} + 2\overline{\alpha}_{30})\\
&\quad + \sin(2\overline{\alpha}_{20} + 2\overline{\alpha}_{30}) + \sin(2\overline{\alpha}_{30})]\\
Q &= -2r^2\omega_{m0}^2[M_1F_1F_2\cos(\gamma_{1x} - \gamma_{2x})\\
&\quad + M_2F_2F_4\cos(\gamma_{2x} - \gamma_{4x})]\\
&\quad + 2r^2[k_{1x}F_1F_2\cos(\gamma_{1x} - \gamma_{2x})\\
&\quad - k_{1x}F_1F_4\cos(\gamma_{1x} - \gamma_{4x}) + k_{1x}F_2F_4\cos(\gamma_{2x} - \gamma_{4x})\\
&\quad + k_{2x}F_2F_4\cos(\gamma_{2x} - \gamma_{4x}) - k_{1x}F_2^2]
\end{aligned}$$

$$
\begin{aligned}
P = & -2r^2\omega_{m0}^2[M_1F_1F_2\sin(\gamma_{1x}-\gamma_{2x}) \\
& + M_2F_2F_4\sin(\gamma_{2x}-\gamma_{4x})] \\
& + 2r^2[k_{1x}F_1F_2\sin(\gamma_{1x}-\gamma_{2x}) \\
& - k_{1x}F_1F_4\sin(\gamma_{1x}-\gamma_{4x}) + k_{1x}F_2F_4\sin(\gamma_{2x}-\gamma_{4x}) \\
& + k_{2x}F_2F_4\sin(\gamma_{2x}-\gamma_{4x})]
\end{aligned}
$$

REFERENCES

[1] S. Orange and N. Verdière, "Nonlinear synchronization on connected undirected networks," *Nonlinear Dyn.*, vol. 76, pp. 47–55, Apr. 2014.

[2] M. Senator, "Synchronization of two coupled escapement-driven pendulum clocks," *J. Sound Vib.*, vol. 291, pp. 566–603, Apr. 2006.

[3] R. Yamapi and P. Woafo, "Dynamics and synchronization of coupled self-sustained electromechanical devices," *J. Sound Vib.*, vol. 285, nos. 4–5, pp. 1151–1170, Aug. 2005.

[4] J. F. Totz, R. Snari, D. Yengi, M. R. Tinsley, H. Engel, and K. Showalter "Phase-lag synchronization in networks of coupled chemical oscillators," *Phys. Rev. E, Stat. Phys. Plasmas Fluids Relat. Interdiscip. Top.*, vol. 92, Aug. 2015, Art. no. 022819.

[5] P. Perlikowski, A. Stefański, and T. Kapitaniak, "1:1 Mode locking and generalized synchronization in mechanical oscillators," *J. Sound Vib.*, vol. 318, pp. 329–340, Nov. 2018.

[6] X. Wang, X. Liu, Y. Shan, Y. Shen, and T. He, "Analysis and optimization of the novel inerter-based dynamic vibration absorbers," *IEEE Access*, vol. 6, pp. 33169–33182, 2018.

[7] B. Xu, C. Xiang, Y. Qin, P. Ding, and M. Dong, "Semi-active vibration control for in-wheel switched reluctance motor driven electric vehicle with dynamic vibration absorbing structures: Concept and validation," *IEEE Access*, vol. 6, no. 1, pp. 60274–60285, 2018.

[8] I. I. Blekhman and E. I. Rivin, *Synchronization in Science and Technology*. New York, NY, USA: ASME Press, 1988.

[9] I. I. Blekhman, *Vibrational Mechanics*. Singapore: World Scientific, 2000.

[10] I. I. Blekhman and V. S. Sorokin, "On the separation of fast and slow motions in mechanical systems with high-frequency modulation of the dissipation coefficient," *J. Sound Vib.*, vol. 329, pp. 4936–4949, Nov. 2010.

[11] I. I. Blekhman, A. L. Fradkov, H. Nijmeijer, and A. Y. Pogromsky, "On self-synchronization and controlled synchronization," *Syst. Control Lett.*, vol. 31, pp. 299–305, Oct. 1997.

[12] B. Wen, J. Fan, C. Zhao, and W. Xiong, *Vibratory and Controlled Synchronization Engineering*. Beijing, China: Science Press, 2009.

[13] J. M. Balthazar, J. L. P. Felix, and R. M. Brasil, "Some comments on the numerical simulation of self-synchronization of four non-ideal exciters," *Appl. Math. Comput*, vol. 164, no. 2, pp. 615–625, May 2005.

[14] J. M. Balthazar, J. L. P. Felix, and R. M. F. Brasil, "Short comments on self-synchronization of two non-ideal sources supported by a flexible portal frame structure," *J. Vib. Control*, vol. 10, no. 12, pp. 1739–1748, 2004.

[15] P. Fang and Y. Hou, "Synchronization characteristics of a rotor-pendula system in multiple coupling resonant systems," *J. Mech. Eng. Sci.*, vol. 232, no. 10, pp. 1802–1822, 2017.

[16] X. Zhang, B. Wen, and C. Zhao, "Synchronization of three non-identical coupled exciters with the same rotating directions in a far-resonant vibrating system," *J. Sound Vib.*, vol. 332, no. 9, pp. 2300–2317, Apr. 2013.

[17] X. Zhang, C. Li, Z. Wang, and S. Cui, "Synchronous stability of four homodromy vibrators in a vibrating system with double resonant types," *Shock Vib.*, vol. 2018, Dec. 2018, Art. no. 9641231.

[18] X. Zhang, B. Wen, and C. Zhao, "Theoretical study on synchronization of two exciters in a nonlinear vibrating system with multiple resonant types," *Nonlinear Dyn.*, vol. 85, no. 1, pp. 141–154, Jul. 2016.

[19] X. Zhang, B. Wen, and C. Zhao, "Vibratory synchronization transmission of a cylindrical roller in a vibrating mechanical system excited by two exciters," *Mech. Syst. Signal Process.*, vol. 96, pp. 88–103, Nov. 2017.

[20] Y. Yang, R. Fu, and L. Huang, "Robust analysis and synthesis for a class of uncertain nonlinear systems with multiple equilibria," *Syst. Control Lett.*, vol. 53, pp. 89–105, Oct. 2004.

XUELIANG ZHANG was born in 1978. He received the Ph.D. degree from Northeastern University, Shenyang, China, in 2014, where he is currently an Associate Professor with the School of Mechanical Engineering and Automation. He has authored over 20 papers in international journals and applied for more than 20 Chinese patents. His research interests include synchronization theory, vibration utilization and control engineering, and nonlinear vibrations in engineering.

ZHIHUI WANG received the bachelor's degree in mechanical design and manufacturing and automation from Yanshan University, Qinhuangdao, China, in 2017. He is currently pursuing the master's degree with Northeastern University, Shenyang, China. His research interests include synchronization theory and vibration utilization engineering.

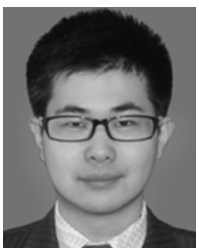

YUNPENG ZHU received the B.S. and M.S. degrees in mechanical engineering and automation from Northeastern University, Shenyang, China, in 2013 and 2015, respectively. He is currently pursuing the Ph.D. degree with the Department of Automatic Control and System Engineering, Sheffield University, U.K. His research interests include the analysis and design of nonlinear systems.

JINLIN XU was born in 1993. He received the bachelor's degree in mechanical design, manufacturing and automation from the Taiyuan University of Technology, Shanxi, China, in 2015, and the master's degree in mechanical engineering from Northeastern University, China, in 2018. His research interests include synchronization theory and vibration utilization engineering.

BANG-CHUN WEN was born in 1930. He received the degree from Northeastern University, Shenyang, China, where he is currently a Professor. He has published over 700 scientific papers, indexed by SCI, EI, and ISTP more than 260, in journals and conferences at home and abroad and over 80 monographs. His research interests include vibration utilizing engineering, synchronization theory of vibrating system, nonlinear vibrations in engineering, rotors dynamics, comprehensive design theory, and method of mechanical products. Especially, in recent years, he proposed scientific methodology with unique features first in the world. He first set up and developed the subject of vibration utilizing engineering. He is a member of the Chinese Academy of Sciences (CAS), International Federation for the Promotion of the Mechanisms and Machine Science (IFToMM) the China Committee, the International Committee for Rotor Dynamics, and the Asia-Pacific Vibration Conference Instruction Committee; the Honorary President of the Chinese Mechanical Engineering Society; the Honorary Director of the Academic Committee of State Key Laboratory of Vibration, Shock and Noise, Shanghai JiaoTong University; and the President of the Chinese Vibration Engineering Society.